Verification of Typhoon Forecasts for a 20 km-mesh High-Resolution Global Model

Hiroyuki MURAKAMI

Advanced Earth Science and Technology Organization (AESTO), Japan Meteorological Agency, Tokyo, Japan

Takayuki MATSUMURA[1], Ryota SAKAI

Numerical Prediction Division, Japan Meteorological Agency, Tokyo, Japan

Akira NODA[2] and Shoji KUSUNOKI

Climate Research Department, Meteorological Research Institute, Tsukuba, Japan

(*Manuscript received 26 March 2007, in final form 11 June 2008*)

Abstract

In this study, twelve tropical storms between 2002 and 2005 over the western North Pacific Ocean, namely, typhoons, were simulated through medium-range forecast experiments with the 20 km-mesh Japan Meteorological Agency (JMA) and Meteorological Research Institute (MRI) Atmospheric General Circulation Model (JM-AGCM). These simulations were compared with the 60 km-mesh JMA Global Spectral Model (GSM) to evaluate differences in resolution. They are verified with the best-track data as an observation. The verification was conducted in terms of estimating error of position, intensifying tendency, radius of 50 knot, 30 knot, and composite wind profile. This paper addresses the importance of such high resolution to predict typhoon's intensity and inner-core structure.

As a result, the JM-AGCM shows slightly smaller position error than the GSM. Moreover, much improvement was seen in the intensity prediction. The JM-AGCM outstandingly can both decrease the central sea level pressure and increase maximum wind velocity, while the GSM can not simulate them because of low resolution. The JM-AGCM also shows better intensifying and decaying tendency than the GSM.

The verifications of 50 knot and 30 knot radii, and the composite wind profile indicate that the typhoon structure by the JM-AGCM is quite realistic. Moreover, the JM-AGCM expresses the drastic transformation of inner-core wind profile within 100km from the typhoon center more realistically than the GSM. These results indicate that a high resolution global model, such as 20 km-mesh, is vital when discussing the intensity and wind profile of tropical storms.

Corresponding author and present affiliation: Hiroyuki Murakami, Advanced Earth Science and Technology Organization (AESTO), Climate Research Department, Meteorological Research Institute, (MRI), 1-1, Nagamine, Tsukuba-shi, Ibaraki 305-0052, Japan
E-mail: himuraka@mri-jma.go.jp

1 Present affiliation: Administration Division, Forecast Department, Japan Meteorological Agency, Tokyo, Japan
2 Present affiliation: Global Environment Modeling Research Program, Frontier Research Center for Global Change (FRCGC), Japan Agency for Marine-Earth Science and Technology (JAMSTEC), Kanagawa, Japan

1. Introduction

A tropical cyclone is one of the most harmful weather phenomena. In Japan, 10 typhoons caused disastrous damage in 2004 (Levinson 2005). Recently, Hurricane Katrina caused catastrophic damage in the United States of America (Schmidlin 2006). These disasters arouse public interest about the relationship between the number or intensity of tropical cyclones and global warming. A number of studies have been conducted to project future climate associated with warmer sea surface temperature (SST) using increased-CO2 scenarios and a global circulation model (GCM) (Broccoli and Manabe 1990; Haarsma et al. 1993; Bengtsson et al. 1996; Krishnamurti et al. 1998; Royer et al. 1998; Shapiro and Goldenberg 1998; Houghton et al. 2001; Sugi et al. 2002; Tsutsui 2002) and regional nested models (Knutson et al. 1998; Knutson and Tuleya 1999; Walsh and Ryan 2000; Knutson and Tuleya 2004). These simulation results, however, are not consistent in the projection of an increase or decrease in the total number of tropical cyclones, although most of the simulations project an increase in the intensity of tropical cyclones. As Henderson-Sellers et al. (1998) warn, however, results by GCM simulations are greatly limited by the coarse resolution of the current GCMs. Indeed, Hamilton and Hemler (1997) showed a simulation in which a strong typhoon (906 hPa in the minimum sea level pressure and peak wind speed 70.5 m s^{-1}) was simulated with a high-resolution model (roughly 35km-mesh). However, as seen in their simulations, only a few simulations have been conducted because of lack of computer resources. Therefore, providing statistical confidence is a Herculean task at this time. Webster et al. (2005) also reported a large increase in the number and proportion of intense tropical cyclones were seen by analysis of best track data. However, as Landsea et al. (2006) pointed out, there are uncertainties to discuss the trend of tropical storm activity through the satellite database because it contains various biases. Therefore both modeling and observation seem to be limited to get reliable information about a trend of tropical cyclone at this time.

However, recent advances in computational resources, such as the Earth Simulator (ES), which is a parallel-vector supercomputer consisting of 5,120 processors (Habata et al. 2004) and the fastest computer in the world (at least at the time this study was started), enable us to project future climate with a high-resolution atmospheric general circulation model (AGCM). Using the ES, the Advanced Earth Science and Technology Organization (AESTO), the Meteorological Research Institute (MRI), and the Numerical Prediction Division of the Japan Meteorological Agency (JMA) have developed a super high-resolution (TL959L60; triangular truncation 959 with the linear Gaussian grid which is equivalent to 20km-mesh horizontally and 60 layers vertically) AGCM (Mizuta et al. 2006; hereafter referred to as "JM-AGCM") to investigate the effect of global warming on typhoons (Oouchi et al. 2006) and Baiu (Kusunoki et al. 2006) under the Intergovernmental Panel on Climate Change (IPCC) scenarios. In particular, Oouchi et al. (2006) showed that the number of tropical cyclones is globally reduced and the number of strong tropical cyclones is increased in the warm-climate environment more than in the present-day climate. Their results support past studies conducted with the low-resolution GCMs (e.g., Bengtsson et al. 1996; Sugi et al. 2002) and seem to be much more reliable than those of other past studies conducted with the low-resolution GCMs. This is because a low-resolution GCM, which is typically 100 kilometers mesh, is too coarse to represent the typical inner structures of a tropical cyclone. Oouchi et al. (2006) carefully evaluated the reliability of their projection by comparing their present-day 10-year experiment with observation with respect to geographical distribution, frequency, and intensity. Although they insist that their 20km-mesh AGCM is more excellent than other coarse model in the intensity forecast of the typhoon, there is no remark of experiments that compares the typhoon structure by the resolutions. Even in the medium-range forecast, there is no research that statistically shows the superiority of such a high-resolution global model from the viewpoint of the typhoon prediction. It should be stressed here that forecast experiments on typhoon position and strength using such a high-resolution AGCM have not been carried out in other numerical prediction centers in the world. Some studies have shown that the tropical storm structure was well simulated with high-resolution AGCMs. For example, Ohfuchi et al. (2004) simulated tropical cyclones as an initial value problem with a 10km-mesh AGCM, which is the highest-resolution AGCM in the world. However, because their simulations were not validated, it is uncertain whether or not their simulated tropical storms

were realistic. Shen et al. (2006) also simulated Hurricane Katrina with a 0.125° grid mesoscale-resolving finite-volume GCM. Although they showed that a high-resolution model provides better intensity forecasts than low-resolution one, only one initial case was shown, and other initial cases are unknown. Therefore, it is important to verify the simulations of targeted real tropical cyclones to determine whether or not they are realistic so as to not only validate the climate simulations but also improve the physical process of the model.

This study aims to statistically evaluate the predictability of tropical cyclone by the JM-AGCM in terms of tracks, intensity, and structure of wind profile through medium-range forecasts. Twelve tropical cyclones over the western North Pacific Ocean, namely, typhoons, were simulated with the JM-AGCM. They were compared with the simulations produced by the 60km-mesh JMA former operational global spectral model (hereafter referred to as "GSM").

Section 2 describes the experimental design containing the forecast models, initial conditions, simulated typhoons, best-track data, and method used to detect the typhoon position. Section 3.a shows the results of position errors. A verification of the intensity and typhoon structure follows in Section 3.b and Section 3.c, respectively. A summary and concluding remarks are presented in Section 4.

2. Experimental design

a. Forecast models

A brief introduction of the JM-AGCM is described here. The JM-AGCM has been developed by the JMA and the MRI for both weather forecasting and climate research. The JMA had used the low-resolution version (TL319L40; triangular truncation 319 with the linear Gaussian grid which is equivalent to 60km-mesh horizontally and 40 layers vertically) of the model as the operational global medium-range forecast since February 17, 2005. Recently the JMA upgraded its resolution as TL959L60, which is the same resolution as our experiments. This model has also been used for future climate projections (Mizuta et al. 2006; Kusunoki et al. 2006; Oouchi et al. 2006). Some descriptions of this model are available in some articles and books (climate mode: Kusunoki et al. 2006; Mizuta et al. 2006; Oouchi et al. 2006, forecast mode: JMA 2007; Murakami and Matsumura 2007). The JM-AGCM adopts a semi-Lagrangian scheme (Yoshimura and Matsumura 2003) which enables integration with a longer time step without being constrained by the Courant-Fredrichs-Lewy (CFL) condition. As a cumulus convection scheme, which is important for typhoon formation, a prognostic Arakawa and Schubert (1974) scheme is implemented. The level 2 turbulence closure scheme of Mellor and Yamada (1974) is used to represent the vertical diffusion of the momentum, heat, and moisture. The resolution of the model is TL959L60, namely, horizontal 20km-mesh and 60 vertical layers. The model employs a sigma-pressure hybrid coordinate as the vertical coordinate (Simmons and Burridge 1981). The model top is placed at approximately 0.1 hPa pressure level, whereas the lowest level is placed at 998.5 hPa pressure level when the surface pressure is 1000 hPa. There are 13 vertical layers below the 800 hPa pressure level and 29 layers over the 200 hPa pressure level. The model is optimized for the ES (Katayama et al. 2003; Katayama et al. 2004). The execution time of the 24-hours forecast is about 6 minutes using 60 nodes of the ES.

Typhoon simulations of the JM-AGCM are compared with those of the JMA former operational global spectral model (GSM). Details on the GSM are available in JMA (2002). The dynamics of the GSM is an Eulerian form. The resolution of the GSM is T213L40, namely, triangular truncation 213 which is equivalent to about 60km-mesh horizontal grids and vertical 40 layers.

Some physical processes in the forecast mode of the JM-AGCM are slightly different from those of the GSM. They are optimized for the medium-range forecast as described in Murakami and Matsumura (2007). The JM-AGCM has adopted recent revision shown in Table 1.

For the GSM simulations, outputs by the JMA operational routine are used. Hence, the GSM only adopts the revisions in Table 1 at the time the typhoon was predicted (e.g., the GSM does not adopt all the revisions for the 2002 typhoon simulation cases, whereas the JM-AGCM adopts them all). However, as Mizuta et al. (2006) pointed out, most of the settings in the physical parameterizations were tuned at the original resolutions of 60km-mesh. Some parameters in some physical processes were adjusted in their climate simulation for convenience, although they were not well verified. It is also uncertain that these adjustments yield good results for a simulation in a forecast mode. Therefore, these adjustments were not applied for the JM-AGCM simulations in this study.

Table 1. List of recent major revisions in the physical processes.

Date	Upgrade	Reference
28 May 2003	Improved cumulus convection scheme including the entrainment and detrainment effects between the cloud top and the cloud base in convective downdraft.	Nakagawa (2003)
29 Jul 2004	A simple parameterization scheme for marine stratocumulus.	Kawai and Inoue (2006)
29 Jul 2004	Improved cloud water/ice scheme.	Kawai (2003)
02 Dec 2004	A new long-wave radiation scheme.	Murai and Yabu (2005)

b. Initial condition

A medium-range forecast experiment is an initial condition problem. Therefore, using appropriate initial data is necessary for medium-range forecasts to avoid a spin-up problem. Although it would appear to be better to use a data assimilation system for the above reason, the high resolution of the JM-AGCM makes it difficult to construct a data assimilation system because of lack of computer resources when this study was launched. Hence, the initial condition was obtained by interpolation from the 60km-mesh JMA Global Analyses (JMA 2002) (GANAL) to the 20km-mesh grids. The typhoon structure in the original GANAL is changed into a somewhat blunt structure compared with the realistic typhoon structure so that the 60km-mesh GSM can resolve it. Therefore, a typhoon bogus insertion within the initial field (Iwasaki et al. 1987; Ueno 1995; JMA 2002) was implemented to reproduce the suitable strength of tropical cyclone-like vortices so that the JM-AGCM can resolve at the high resolution. Figure 1 shows an example of the typhoon bogus implantation. (a) of Fig. 1 displays the initial typhoon structure of an original GANAL. The central pressure is 992.19 hPa, which is much higher than the 960 hPa of the best-track data (the best-track data will be described in Section 2.d). On the other hand, (b) of Fig. 1 shows the initial field with the typhoon bogus for a 20km-mesh model. The central pressure of the typhoon is 973.77 hPa, which is closer to the best-track data than the original GANAL. Although the typhoon bogus creates typhoon vortex quite realistically, the vortex does not seem to be exactly adjusted for the JM-AGCM. Kurihara et al. (1993) and Bender et al. (1993) pointed out that an insufficient initial typhoon vortex leads to a false spin-up for the first one or two days to adjust the initial typhoon structure by a finer resolution model; similarly, our forecast experiments with the typhoon bogus also showed a false spin-up in the early forecast stage, which was remarkably observed with intensity.

However, some preliminary experiments confirmed that typhoon forecasts with the bogus are superior to those without it in terms of intensity and position error. Hence, the typhoon bogus was applied in this study. To avoid such a spin-up, Kurihara et al. (1993) introduced an optimum initialization system to generate a vortex which is compatible with the physics and the high-resolution model. However, improving the typhoon vortex in the initial condition is beyond the scope of this study and will be a challenging task for the future. Nevertheless, noise in an initial field, which is mainly caused by interpolation errors, cannot be negligible (see Fig. 14 in Murakami and Matsumura (2007)). In order to remove the noise, our preliminary study (Murakami and Matsumura 2007) succeeded in developing an effective nonlinear normal-mode initialization method for a high-resolution AGCM; thus, a medium-range forecast with the AGCM becomes feasible. Figure 2 shows the overall experimental configuration for the typhoon forecasts for the JM-AGCM. The initial time of the forecast is 4 times a day (00, 06, 12, and 18 UTC). The initial data is obtained by interpolation from the 60km-mesh GANAL, as mentioned above (see broken line in Fig. 2). The time integration for each forecast is carried out for 96 hours. A deterministic 6-hour forecast during the 96-hour forecast was used for the incremental normal-mode initialization (Ballish et al. 1992; Murakami and Matsumura 2007) at the next initial time (see box marked as "Guess" in Fig. 2).

The output of simulations by the GSM is available by 90 hours. Basically, the output of the JMA operational routine is available only for forecasts started on 00 UTC and 12 UTC. However, in order

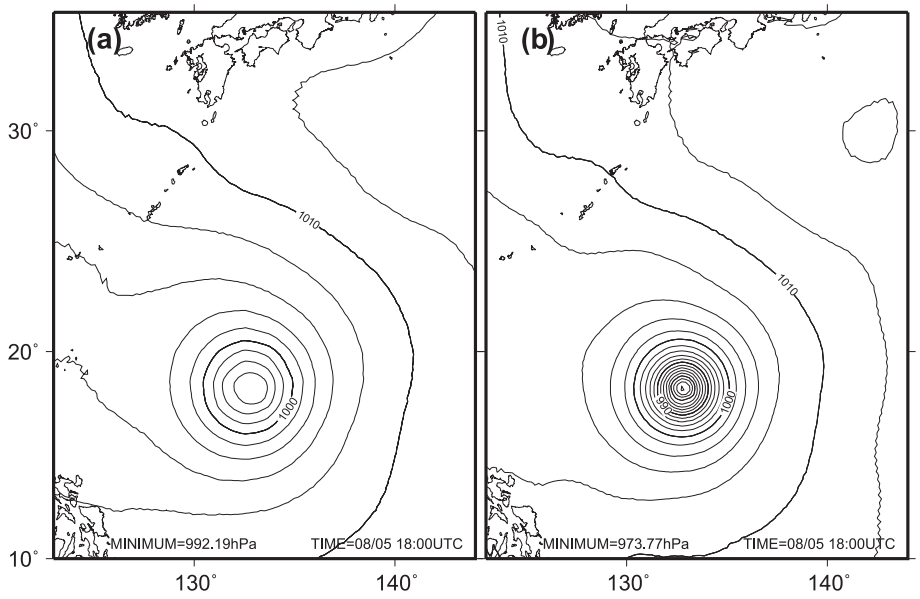

Fig. 1. Typhoon bogus inserted into GANAL. (a) The original GANAL. (b) The 20km-mesh initial field with the typhoon bogus. The central sea level pressure of the original GANAL is 992.19 hPa, whereas that of the 20km-mesh initial field is 973.77 hPa. The best-track data shows 960 hPa at the same time of 18UTC on August 5 of 2003.

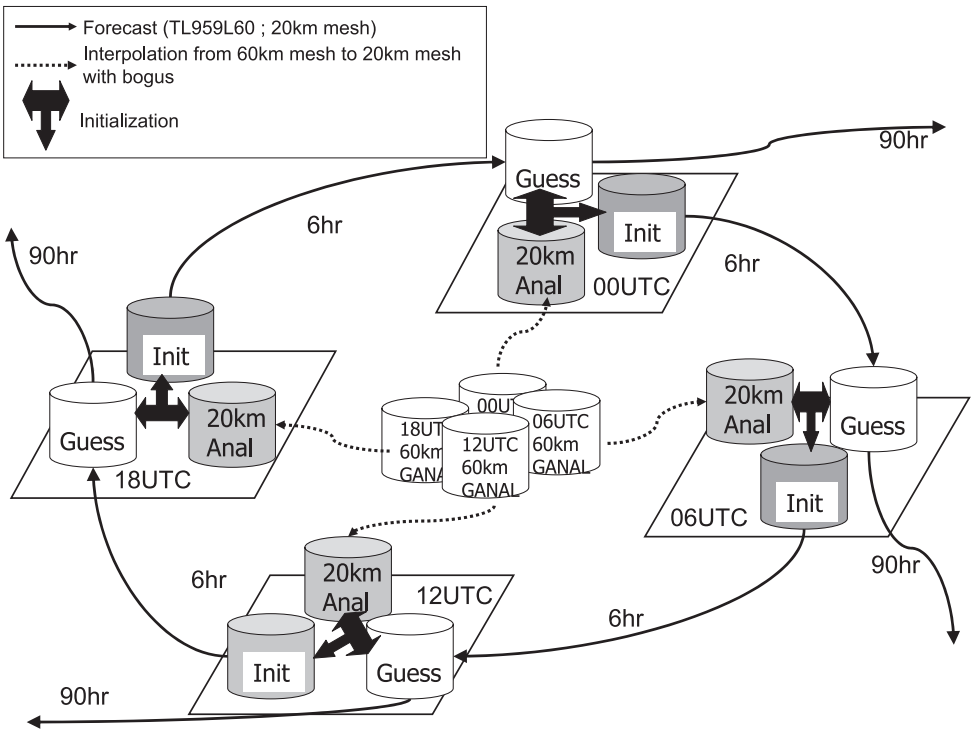

Fig. 2. Configuration of the typhoon experiment. The boxes 60 km GANAL, 20 km Anal, Guess, and Init correspond to the original 60km-mesh analysis, interpolated analysis, first-guess, and initialized data, respectively. The broken line is the interpolation and the typhoon bogus. The thin arrows are deterministic forecasts, and the thick three-pronged arrows are the new initialization scheme.

to gain further statistical confidence, forecasts started on 06 and 18 UTC under the same setting of a routine GSM are implemented. For a homogeneous comparison with the JM-AGCM, simulations within 90 hours are evaluated.

c. Simulated typhoons

Twelve typhoons were selected for verification using the following subjective criteria while considering the limitation of the computational resources given by the ES;

- hazardous typhoons which come close to or land on Japan,
- typhoons that recurve (or never recurve),
- recent typhoons from 2002 to 2005,
- typhoons whose track was well (or badly) predicted by the GSM.

The list of selected typhoons and their experiment periods of initial time are summarized in Table 2. Those forecast dates almost overlap with the period of tropical storms analyzed (TS, when the maximum sustained wind is between 34 knots to 47 knots); severe tropical storm (STS, between 48 knots to 63 knots); and typhoon (TY, over 64 knots) as classified by WMO (2005). The characteristics of each typhoon are well described in JMA (2001–2005).

Table 2. List of all simulated typhoons.

Typhoon Name	Typhoon Number	Number of Cases	Dates of Forecast
Chataan	T0206	48	Jun 29, 2002–Jul 11, 2002
Halong	T0207	38	Jul 07, 2002–Jul 16, 2002
Etau	T0310	25	Aug 03, 2003–Aug 09, 2003
Maemi	T0314	32	Sep 06, 2003–Sep 13, 2003
Dianmu	T0406	34	Jun 13, 2004–Jun 21, 2004
Meranti	T0412	20	Aug 04, 2004–Aug 09, 2004
Songda	T0418	45	Aug 27, 2004–Sep 07, 2004
Meari	T0421	37	Sep 20, 2004–Sep 29, 2004
Ma-on	T0422	23	Oct 04, 2004–Oct 09, 2004
Tokage	T0423	33	Oct 12, 2004–Oct 20, 2004
Talim	T0513	17	Aug 29, 2005–Sep 02, 2005
Nabi	T0514	41	Aug 29, 2005–Sep 08, 2005

d. Best-track data

The simulated track position and intensity are verified with the post-analyzed best-track data distributed by the Regional Specialized Meteorological Center of Tokyo (RSMC-Tokyo), which is managed by the JMA. The data set provides the central position, central pressure, estimated 10 minute-averaged maximum sustained wind speed, and size (e.g., the radius of 30 knots and 50 knots). They are estimated from observations, namely, aircraft, satellite, surface, and upper air observations (Kamahori et al. 2006). In this study, the central position, the central pressure, the maximum 10 minutes-averaged sustained wind speed, and the radii of 30-knot and 50-knot winds in the data set are used as an observation. The radius is analyzed from a center of typhoon in four directions, namely, north, west, south, and east. When all directions of the radius are not missing, the average value is used to compare with the results of simulations.

The best-track data of the simulated typhoons are shown in Fig. 3. In general, except for T0412 and T0513, most typhoons were generated on the south east of the Pacific Ocean approximately between 5°N and 15°N where the SST is high. Then, they moved northwestward while decreasing in central pressure and intensifying the maximum wind. At the time of or just before the recurvature, they reached their peak intensity. After recurvature, they changed their moving direction to northeastward with fast moving velocity and proceeded to disappear.

e. Method to detect the position of a typhoon

The method for detecting the typhoon central position by simulations is the same as the method by Sakai and Yamaguchi (2005) except for the mean sea level pressure (MSLP), for which outputs of 6-hour intervals are used. The method is as follows. At an initial time, the nearest position of the minimum MSLP points from the best-track position is defined as the central point of a typhoon. At 6 forecast hours, the minimum MSLP point within 500 km from the central point at the initial time is defined as the central point. After 12 forecast hours, the minimum MSLP point within 500 km from the point of the linearly extrapolated point by the last 2 forecast positions is defined as the central point. In the case of missing the minimum MSLP point, the tracking is terminated. For homogeneous verification, only samples which are determined by both models are used.

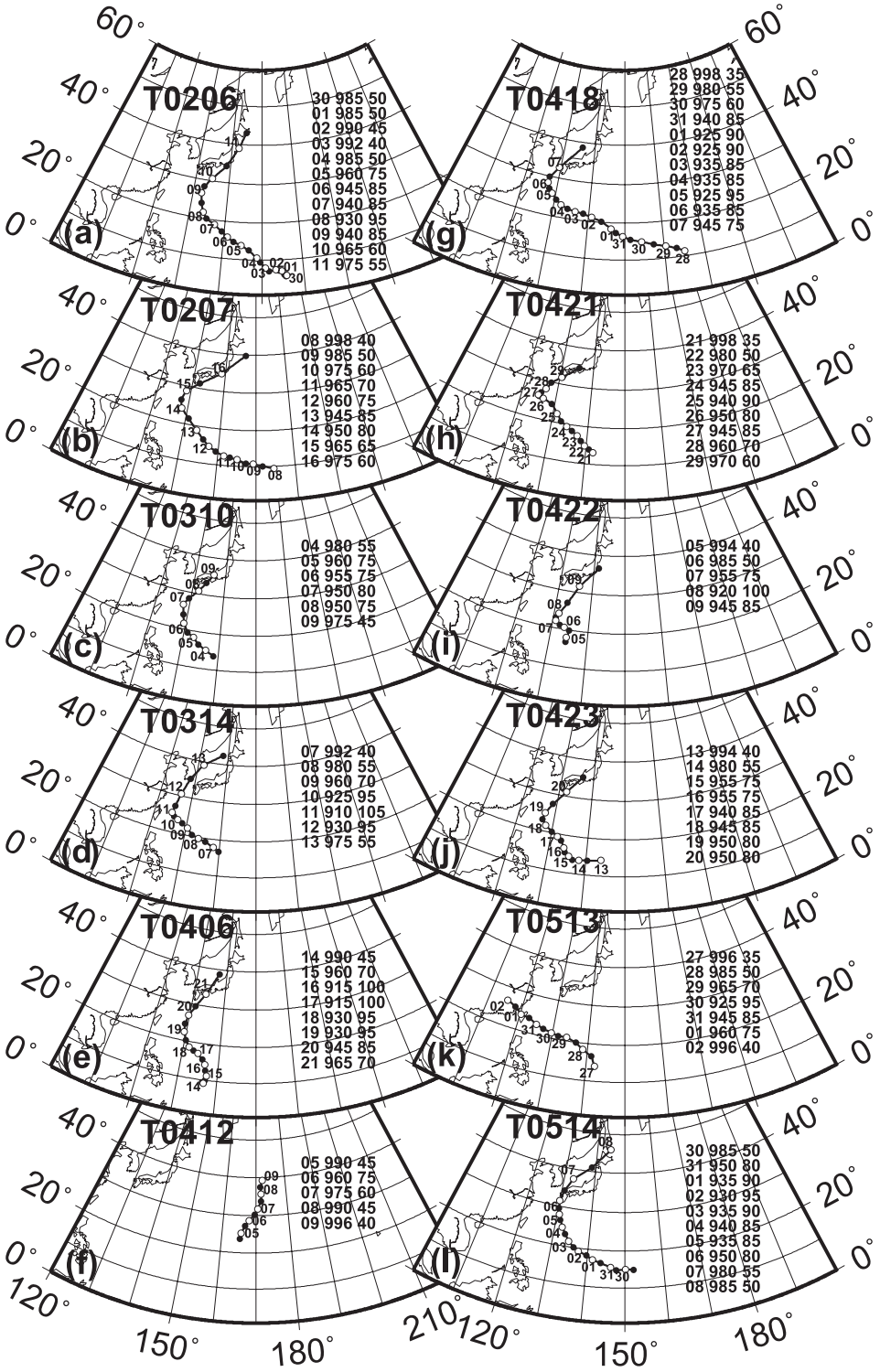

Fig. 3. Best-track data by the RSMC-Tokyo Typhoon Center for (a)T0206, (b)T0207, (c)T0310, (d)T0314, (e)T0406, (f)T0412, (g)T0418, (h)T0421, (i)T0422, (j)T0423, (k)T0513, and (l)T0514. An open circle and a closed circle are the positions at 00 UTC and 12 UTC, respectively. The numbers along the tracks show the date at 00 UTC. The numbers of the right side of each panel describe the date, central sea level pressure (hPa), and maximum sustained wind (knot) from left, respectively.

Radii of 50-knot and 30-knot wind velocity (hereafter R50 and R30) are also derived using 10 m wind components of the model output. The radii are firstly sought for all four directions (i.e., north, east, south, and west) from the center of a storm. When a grid value of 30-knot or 50-knot wind is detected for the first time, it is considered as an inner-core side and ignored because radii of outer-core side are focused here. When the radii are detected for the second time for all directions, they are averaged and compared with the best-track data. If any one radius is not detected, it must become a missing value. Here, in general, the wind speed is weaker on land than on the ocean. This is true for both the observation and simulated results. However, when a storm is close to land, the best-track data consider the land effect. Figure 4 shows an example. The northern positions of the radii are different from each other. When the above detecting algorithm is applied, the radius becomes small because the wind velocity on land is very weak. On the other hand, the radius obtained by the best-track data is from farther to the north. If these differences are not taken into account, a small bias will always be present. To prevent this error, a third point of radius should be considered. However, in this study, the radius points on land were converted to missing data and not used for the analysis; in other words, only radius points on the ocean are evaluated.

3. Results and discussion

a. Position errors

Figure 5 presents all the results of the simulated tracks for the whole of experimental periods. When these results are viewed as a whole, most tracks by the JM-AGCM are very similar to those by the GSM. The westward movement in the early developing stage of T0207, T0310, and T0421 was difficult to predict. The tracks by the JM-AGCM also show a noticeable northward bias in the developing stage. Although the bias of the JM-AGCM is slightly smaller than that of the GSM, it does not seem to be significantly improved by the resolution increase. One of the possible reasons for the northward bias is that the cumulus parameterization scheme in the GSM produces a cold bias at the lower troposphere over the middle and low latitudes (Nakagawa 2003). This leads to a systematic negative error in geopotential height over the western portion of the North Pacific high. It is indicated that the induced weak subtropical high causes a northward bias. Figure 6 shows composite large-scale field for the T0207 cases which is only averaged before the typhoon recurves (BR stage as explained later). It seems that the center

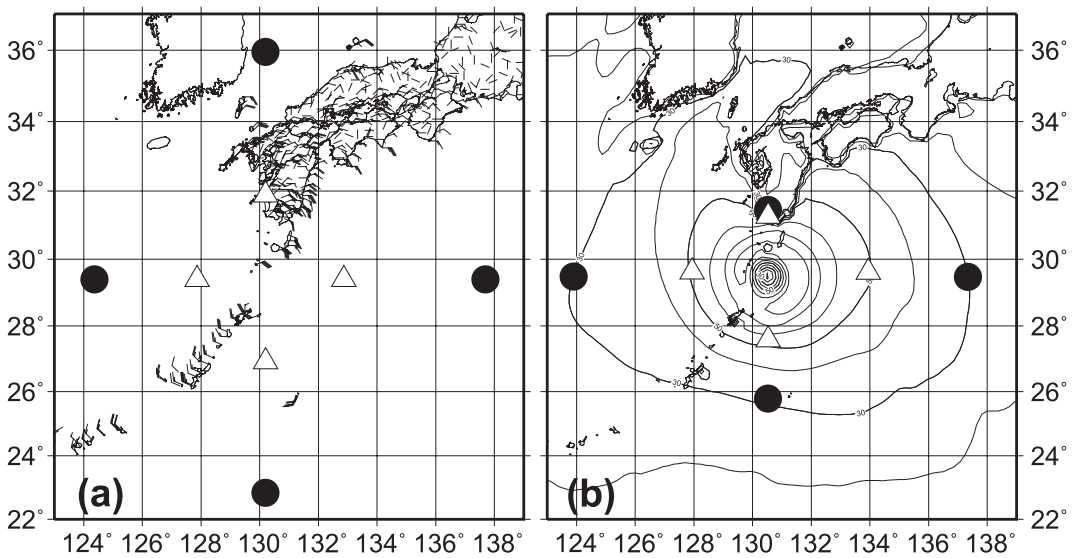

Fig. 4. Land effect on detecting R50 and R30. Position of R50 and R30 (a) by the best-track data and (b) by the JM-AGCM. The winds arrows in (a) are by the Automated Meteorological Data Acquisition System (AMeDAS; one wing is equal to 10 knots). The black circles show the positions of R30, whereas the white triangles show the positions of R50.

of subtropical high shifts westward in the analysis, whereas those by models locate east of the analysis. The notable northward flow bias locates the edge of the subtropical high. It is also fairly obvious that westerly wind bias is seen between 15°N and 20°N latitude for both models. The strong westerly wind bias penetrates far east so that it interrupts westward moving of typhoon. They are caused by the wrong position or the weakness of the subtropical high. There also exists cooling bias around the subtropical high. The degree of the cold bias of the JM-AGCM is less than that of the GSM, which results in smaller northward bias of the storm positions. Nakagawa (2003) pointed out that the cooling bias was alleviated by introducing an improved cumulus parameterization scheme (Table 1). The improved cumulus parameterization scheme is not included in the GSM for the simulation of T0207, but it is in the JM-AGCM. However, the northward bias was not dramatically improved by the JM-AGCM AGCM.

The other possible reason for the northward bias is the inappropriate initial data, mainly due to the lack of observations in the tropical area. Tokuno and Ohhashi (2003) conducted a forecast test with an assimilation using the QuikSCAT wind data for the T0207 typhoon case. They showed that the northward bias is about 100 km reduced with the data. Although detail reasons for the improvement are not clear, they stated that root mean square error of temperature and geopotential height at 850 hPa level and temperature at 500 hPa level are

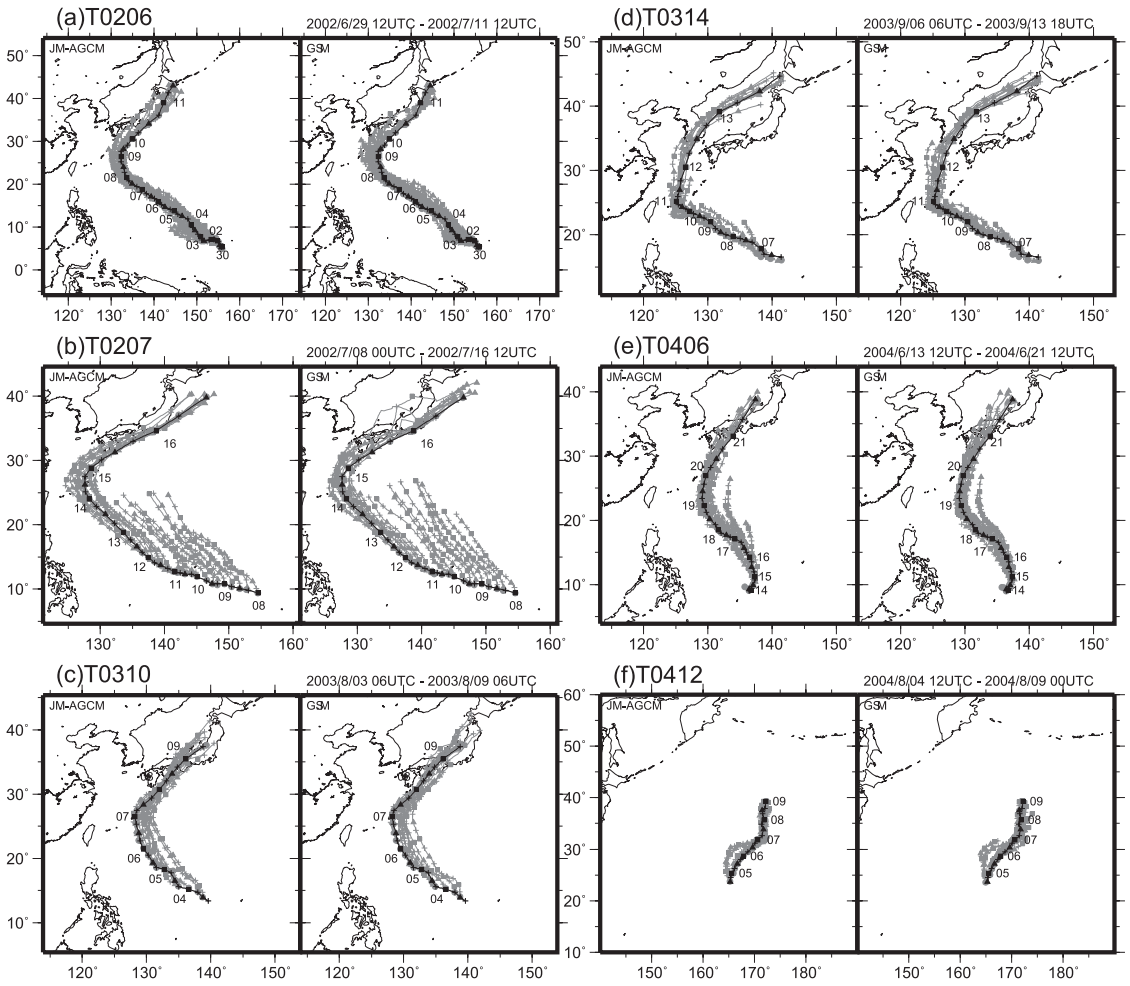

Fig. 5. Simulated typhoon tracks. The left and right panels of each typhoon show the results according to the JM-AGCM and the GSM, respectively. The gray lines are according to the models. The black lines are according to the best-track data. The numerical annotations denote dates.

decreased by the forecast with the QuikSCAT. It is inferred that correcting the errors of the large-scale field is mostly a key for improving northward bias. The GANAL, in which the current study was originally used, was not created using the QuikSCAT data.

Although the wrong timing of the recurvature (T0418, T0421, T0423, and T0514) is notable, the westward bias before the recurvature (T0421) is also remarkable in both models, and the tracks by each model do not seem to be significantly different. Figure 7 is the same as Fig. 6 but for the T0421 case. In this T0421 case, the GANAL shows that the typhoon moves along the edge of subtropical high. Although the models simulate the subtropical high comparatively well in the early forecast hours, they can not simulate the westward propagation of the high-pressure system in the later forecast hours. As a consequence, northwesterly wind goes into the edge so that it interrupts northward moving of typhoon. It is indicated together with the T0207 result that the error of the large scale field as subtropical high leads either northward or southward position error of typhoon systematically.

As for the cases of T0412 and T0513, which never experience recurvature, the track error of the JM-AGCM is almost the same as the GSM or slightly decreased. Because the large-scale field is not so different among models, it is indicated that if the large scale field is almost the same, the position difference between the 20 km model and the 60 km model is not so significant.

Figure 8 shows the statistics of the position error for all typhoon cases in which various typhoon

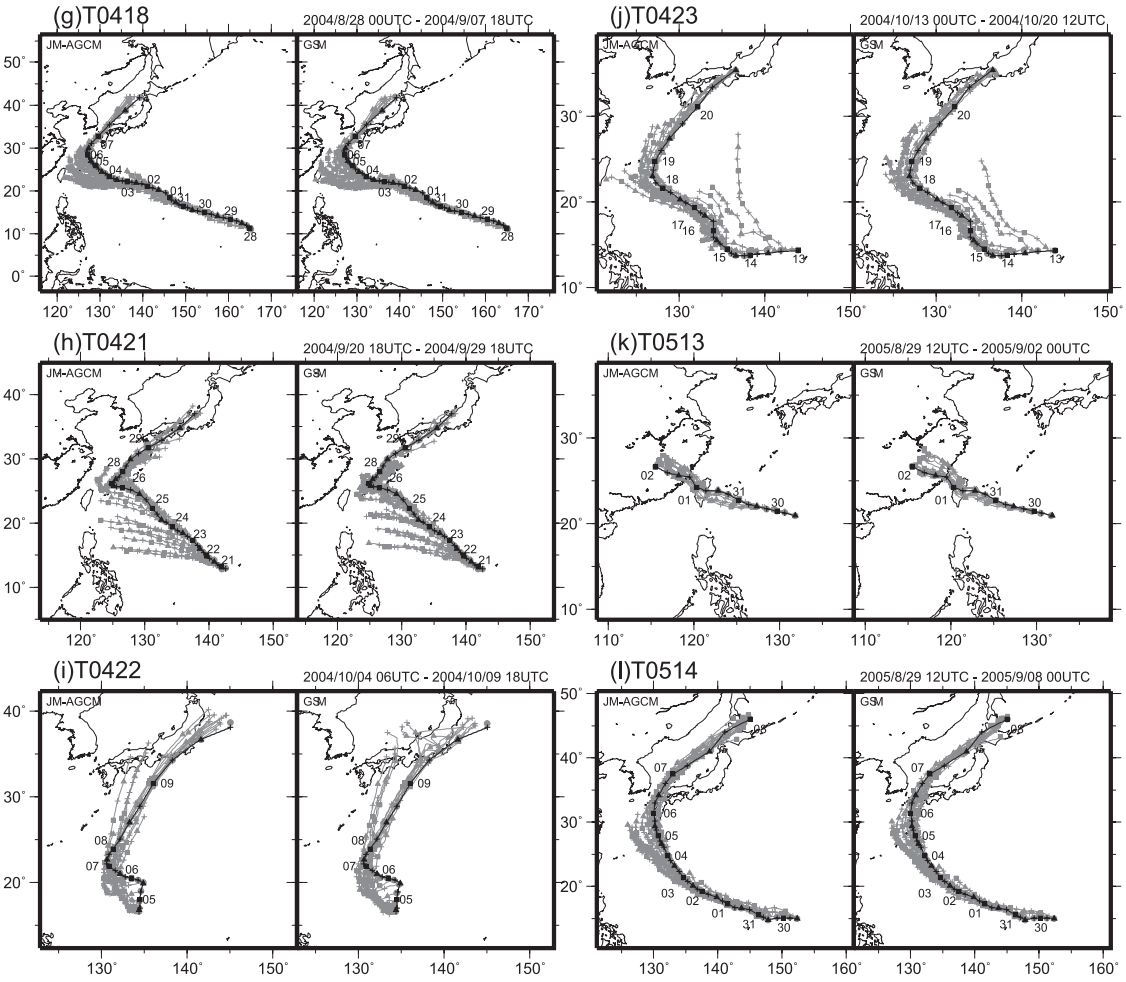

Fig. 5. (continued)

stages are classified. Here, (a) displays the position error of all typhoon cases. All cases are classified according to the storm recurvature as (b) before recurvature (BR); (c) during recurvature (DR); and (d) after recurvature (AR). These recurvature stages are defined by the direction of typhoon motion. The BR is defined as the moving direction of 180–320 degree of the clockwise angle from the north; DR, as 320–10 degrees; and AR, as 10–180 degrees. All cases are also classified according to

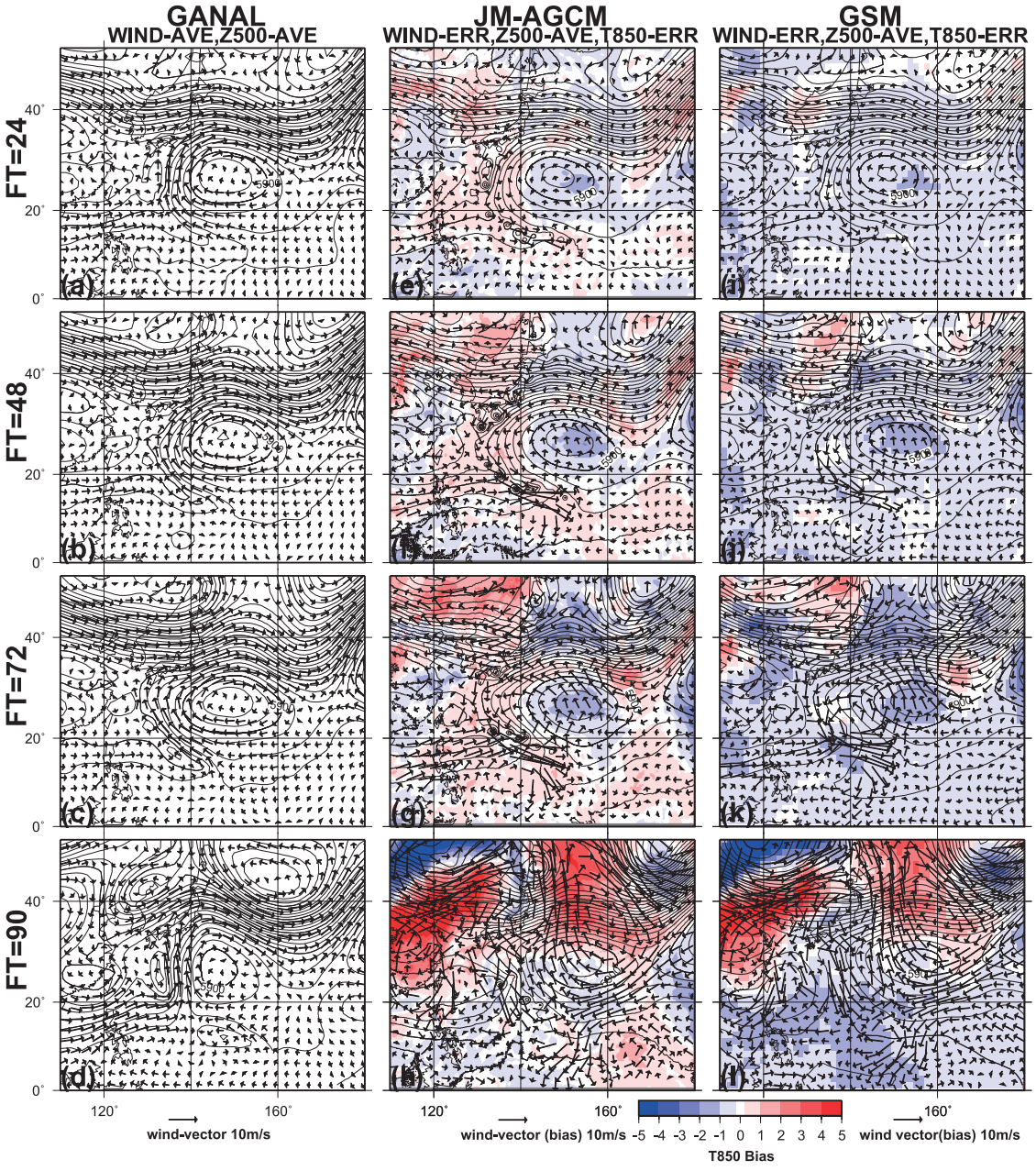

Fig. 6. Composite large-scale field for the T0207 which is averaged before the typhoon recurves. The left panels are averaged analysis field. The contour lines show geopotential height at 500 hPa (Z500). Vectors show weight-averaged wind from 1000 to 300 hPa (WIND). The middle panels are by the JM-AGCM, and the right panels are by the GSM. The contour lines are Z500, the vectors show WIND bias against analysis, and the colors show temperature bias at 850 hPa level.

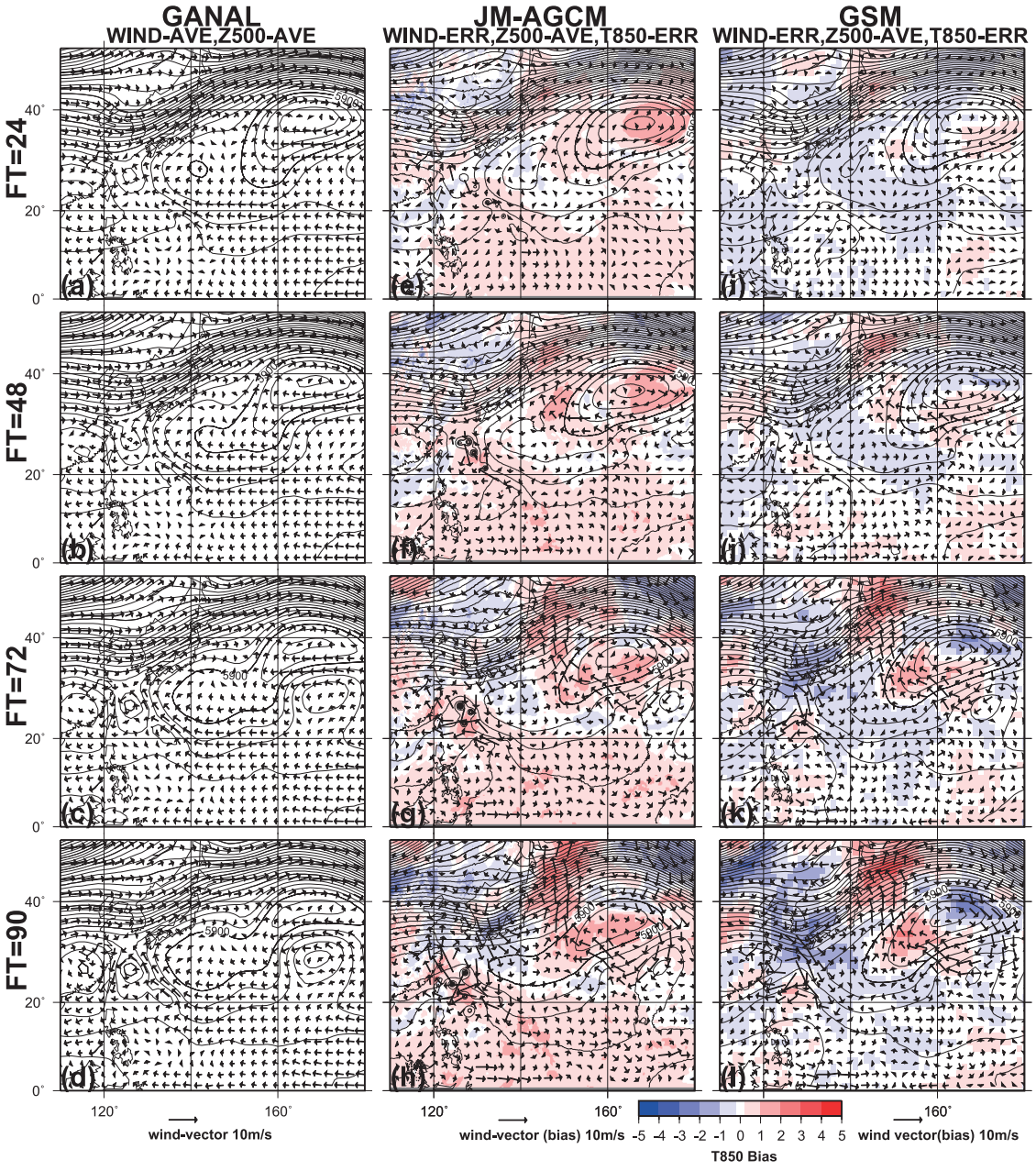

Fig. 7. Same as Fig. 6 but for T0421 case.

the storm intensity, namely, (e) TS, (f) STS, and (g) TY. In general, model differences regarding position error at each forecast hour are not statistically significant because of large variance and lack of sampling cases. The two-sided Student's t-test shows at most 40 percent significance for each hour between models. In spite of the small statistical significance of the model difference, some features can be seen in the figure.

In the early forecast hours, the two models show almost the same track errors for all stages. Approximately after 36 hours, the model difference becomes larger. When typhoons are in the stage of BR and AR, the position error of the JM-AGCM is less than that of the GSM. On the other hand, during the DR stages, the position error of the JM-

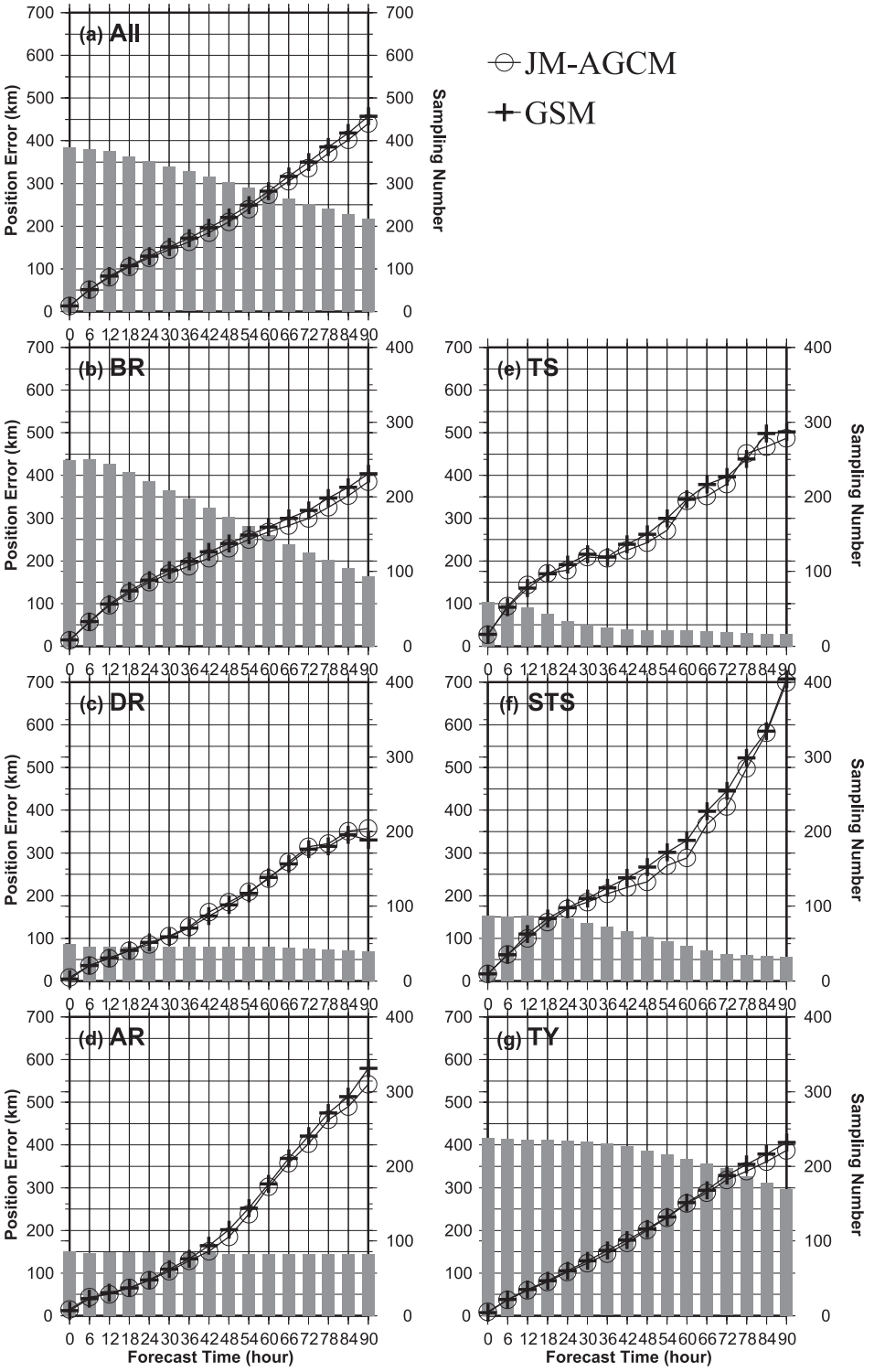

Fig. 8. Simulated position error (km). (a) is the position error for all cases. All cases are classified according to the moving direction as (b) before the recurvature (BR); (c) during the recurvature (DR); and (d) after the recurvature (AR). All cases are also classified according to intensity as (e) TS; (f) STS; and (g) TY. The open-circle plots show the error by the JM-AGCM, and the cross plots show the error by the GSM. The sampling number is shown in the histogram.

AGCM is larger than that of the GSM in the later forecast hours. Because the sampling number is small, it is insufficient to argue that the JM-AGCM causes larger bias at the DR stage. However, a few cases of the systematic larger error were seen in the T0514 simulations. Figure 9 shows an example. Both the JM-AGCM and the GSM could not predict the recurvature. After 24 forecast-hour, the bias of the JM-AGCM becomes larger. Because the large-scale field was not so different between the models (figure not shown), it is indicated that some structure errors of the typhoon generate such bias. As seen in the Fig. 9 case, the JM-AGCM strengthens the typhoon too strong while the analysis does not strengthen. Although the degree of the error by the GSM is less than that of the JM-AGCM, the difference between models and best-track data is large comparatively. The GSM also shows false intense tendency while the best-track data shows steady or slightly decay tendency. It is natural to assume that if typhoon becomes strong, its moving direction becomes difficult to be influenced by the large-scale flow. The reason of this false tendency during the DR stage is uncertain at the moment. One of the possible reasons is that convection in the models is too strong at the early forecast hours to adjust unstable initial field. Then the latent heat release promotes updraft at the center. Once the updraft becomes predominant, much more water vapor at lower levels may be collected at the center and promotes latent heat release. If such a feedback is truly happens in the models, the initial field structure is very critical for correct intensifying tendency. Although it is still uncertain, the key for the precise position prediction of the DR stage might be to correct intensity tendency or typhoon structure.

Evaluating the model difference of the position error by the intensity stages is difficult because most samples are in the TY stage and the sampling numbers for TS and STS are very small. In the TY stage, however, there are small differences of position error between models. Although the statistical significance is low, the JM-AGCM simulates the typhoon positions as realistically as the GSM.

Figure 10 shows a scatter diagram of the position error at 72 forecast hours decomposed into the along/across moving direction relative to the best-track storm position. The ordinate represents the error along the direction the storm is moving, whereas the abscissa represents the error across the direction the storm is moving. Here, three stages are classified as Fig. 8, namely, (a)–(b) BR, (c)–(d) DR, and (e)–(f) AR. During the BR stage,

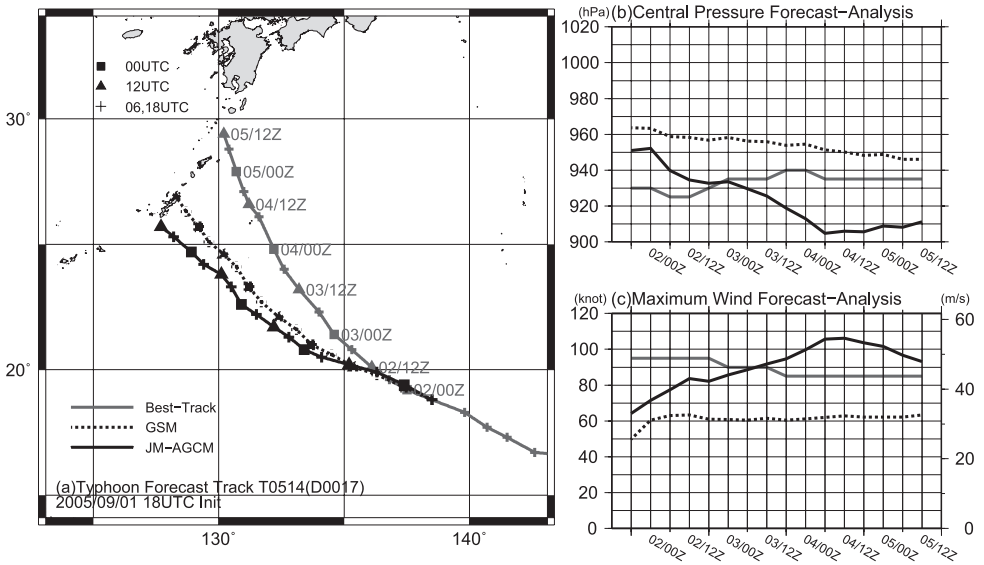

Fig. 9. An example of position error in the DR stage of T0514 case. (a) the typhoon position, (b) the central pressure, and (c) the maximum wind. The black-solid lines are by the JM-AGCM, the black-broken lines are by the GSM, and the gray lines are by the best-track. The initial time is 18UTC on September 5 of 2005.

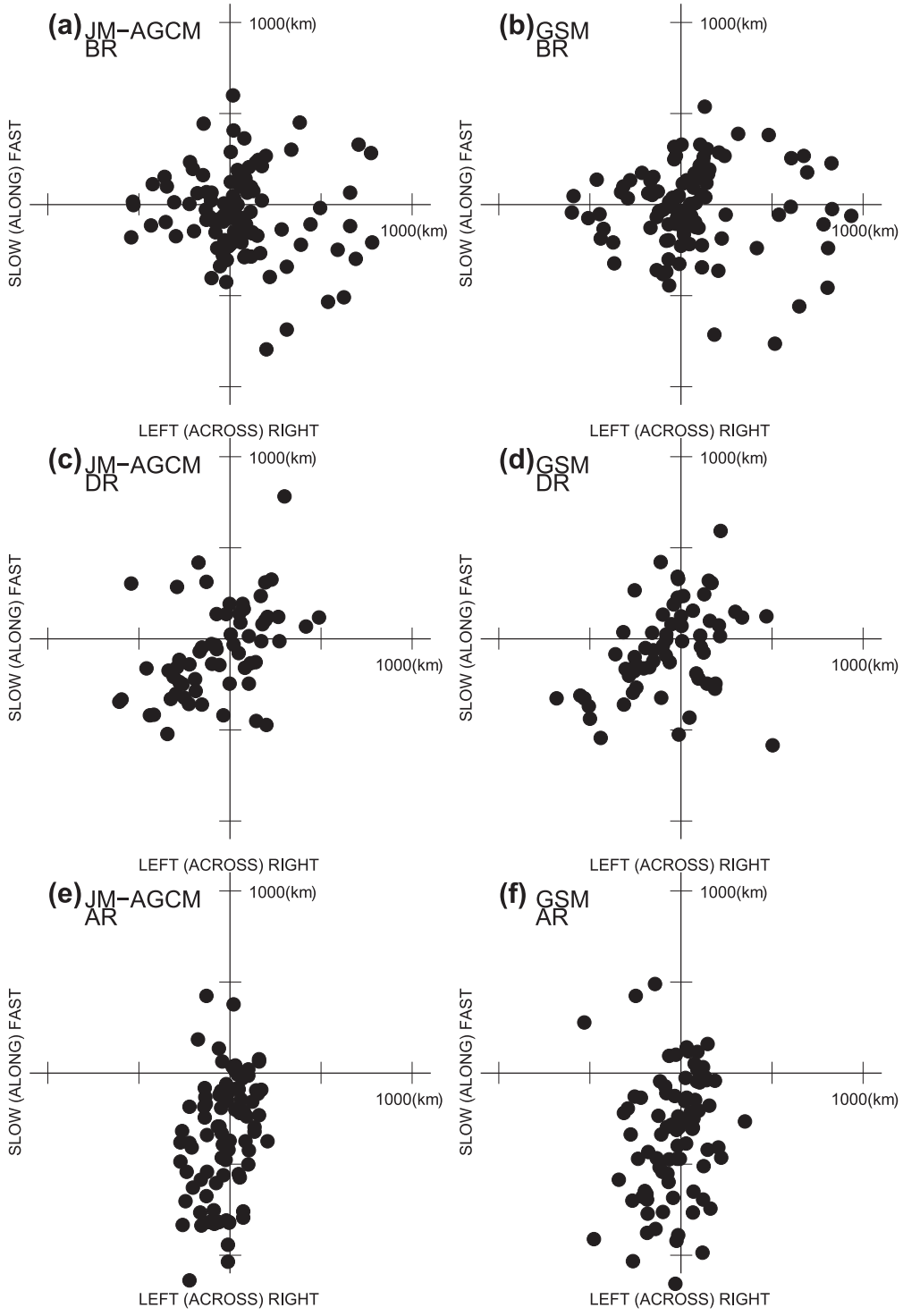

Fig. 10. Simulated central typhoon position along/across the moving direction relative to the storm position of analysis. The typhoon positions at 72 forecast hours are plotted for (a)–(b) as before the recurvature (BR), (c)–(d) during the recurvature (DR), and (e)–(f) after the recurvature (AR) stage. (a), (c), and (e) are according to the JM-AGCM; (b), (d), and (f) are according to the GSM. The abscissa and ordinate represent the error of the across moving direction and the along moving direction, respectively.

the positive errors of the across moving direction (i.e., northward bias) are distinct. Although the positive errors would appear to be mainly due to the T0207 typhoon, as seen in Fig. 5, they are seen in almost every typhoon case. Note that this northward bias in the BR stage is also seen in most operational global models in the world (Wu et al. 2000; Sakai and Yamaguchi 2005). Except for the positive errors, the negative bias is also large in the both models. This bias was remarkable in the case with T0421 as seen in Fig. 7. Overall, the forecasted central position is broadly distributed around the analysis position and not so different among models. As for the DR stage, there are fewer differences among models. When it comes to the AR stage, negative errors along the storm moving direction (i.e., slow bias) are remarkable for both models. Figure 11 shows the scatter diagram as same as the Fig. 10 but for AR stage for each forecast hour. The large slow bias after the recurvature is mainly

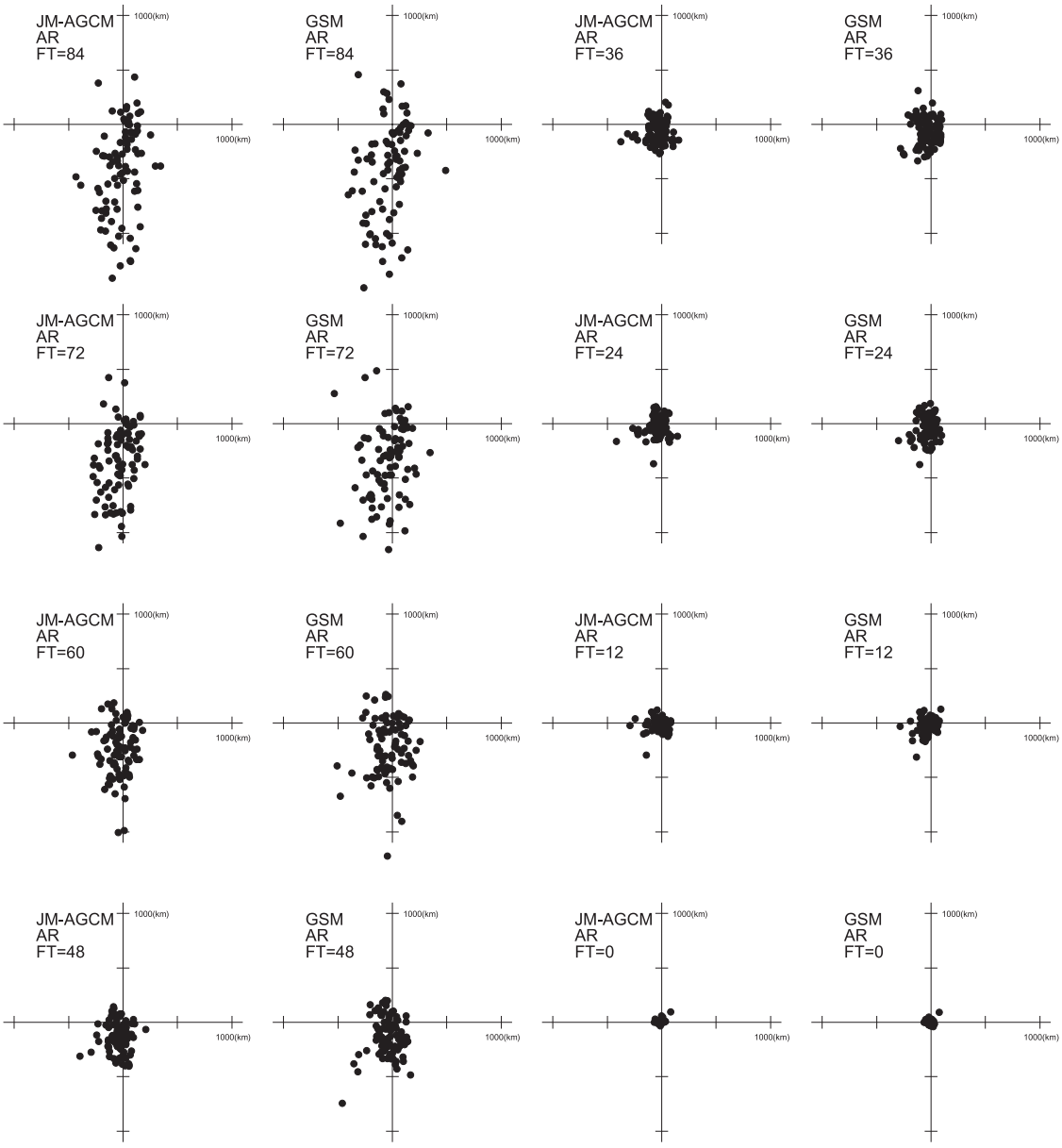

Fig. 11. Same as Fig. 10 but for AR stage for each forecast hour.

notable at the later forecast hours so that it is due to the model error rather than the initial condition error. Figure 12 is the same as Fig. 6 but for the all typhoon cases in the AR stage. It is interested that the cold bias by the both models is seen around the subtropical high and the strength is weaker than the analysis. There also exists warm bias at the north flank of the jet stream around Japan. It is considered that decreasing meridional temperature gradient results in weakening the jet stream by the thermal wind relation. Although there is room for more work to clarify the reason for the warm bias, the slow bias seems to be caused by the error of the weak jet stream.

Figure 13 also shows the distribution of the systematic bias of the mean position (vector) and sea

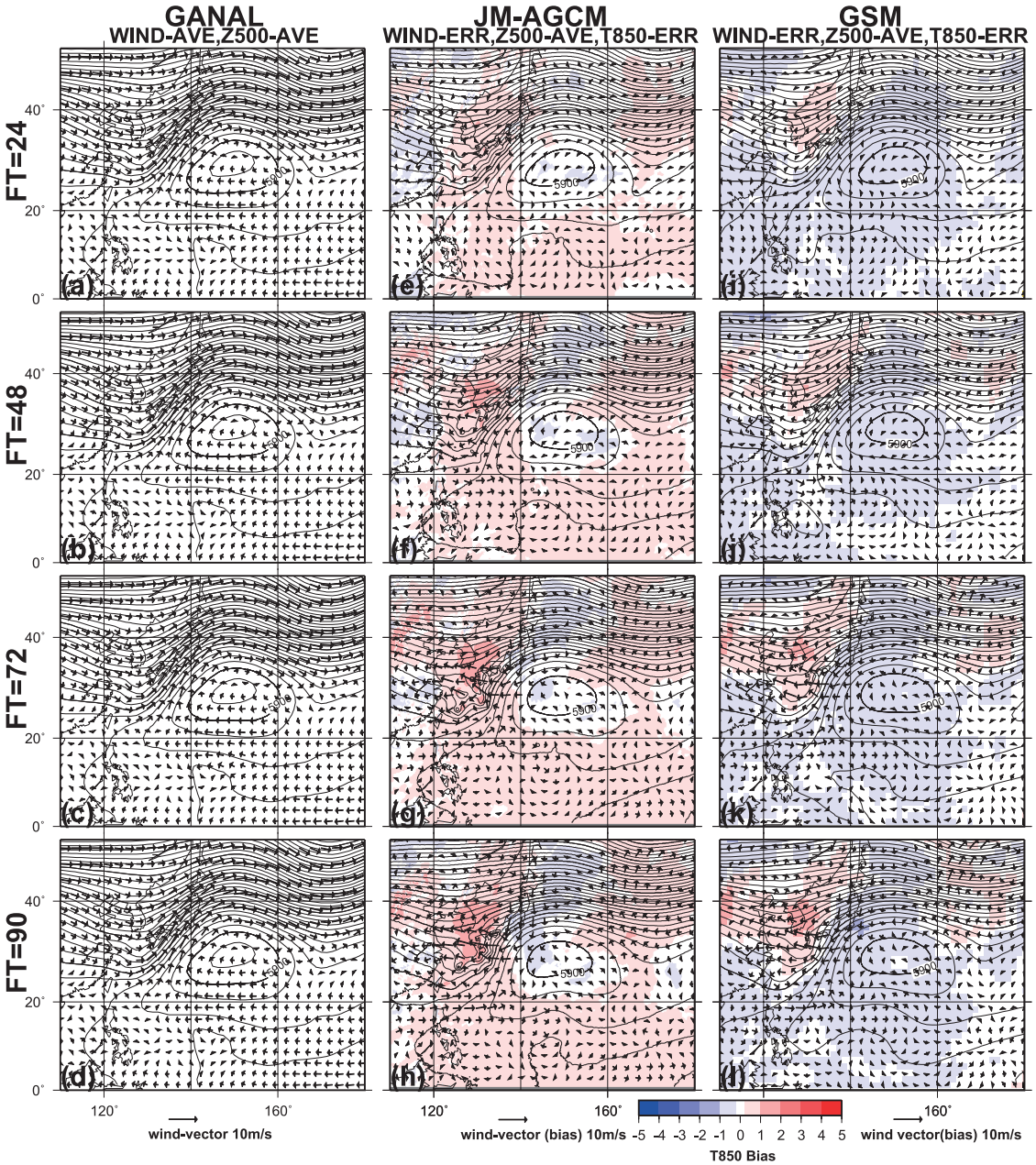

Fig. 12. Same as Fig. 6 but for the all typhoon cases in the AR stage.

level pressure (contour) verified on two-degree grids for the 24 and 72 forecast hours, in which all typhoon cases are averaged. When the biases of position are viewed as a whole (the bias of the sea level pressure will be discussed in Section 3.b), the bias in the 24 forecast hours is clearly less than that in 72 forecast hours. Furthermore, both models show quite similar patterns of erroneous direction and magnitude at 24 forecast hours. There exists a general northward bias in the region south of 20°N and between 125°E and 155°E at both of 24 and 72 forecast hours in both models. This indicates that a typhoon tends to go northward before recurvature, as is already pointed out in Fig. 10. There also exists a large southward or southwestward bias in the region north of 25°N. This indicates that the typhoon tends to move slowly after recurvature, as is also pointed out in Fig. 10.

Overall, both models simulate storm tracks quite similarly. Furthermore, they share systematic northward and southward biases before recurvature and slow bias after recurvature. The fact that the difference of the simulated track between the JM-AGCM and the GSM is small indicates that a refining resolution is not the only key to reduce track errors.

b. Intensity verification

The typhoon intensity, namely, the central pressure and maximum sustained wind, is compared between models.

Figure 14 and Fig. 15 show the simulated central pressure and maximum sustained wind, respectively. When viewed as a whole, the GSM predicts both the central pressure and maximum wind too weakly, while the JM-AGCM predicts them as strongly as, or stronger than, the best-track data. In particular, the variance of the JM-AGCM seems

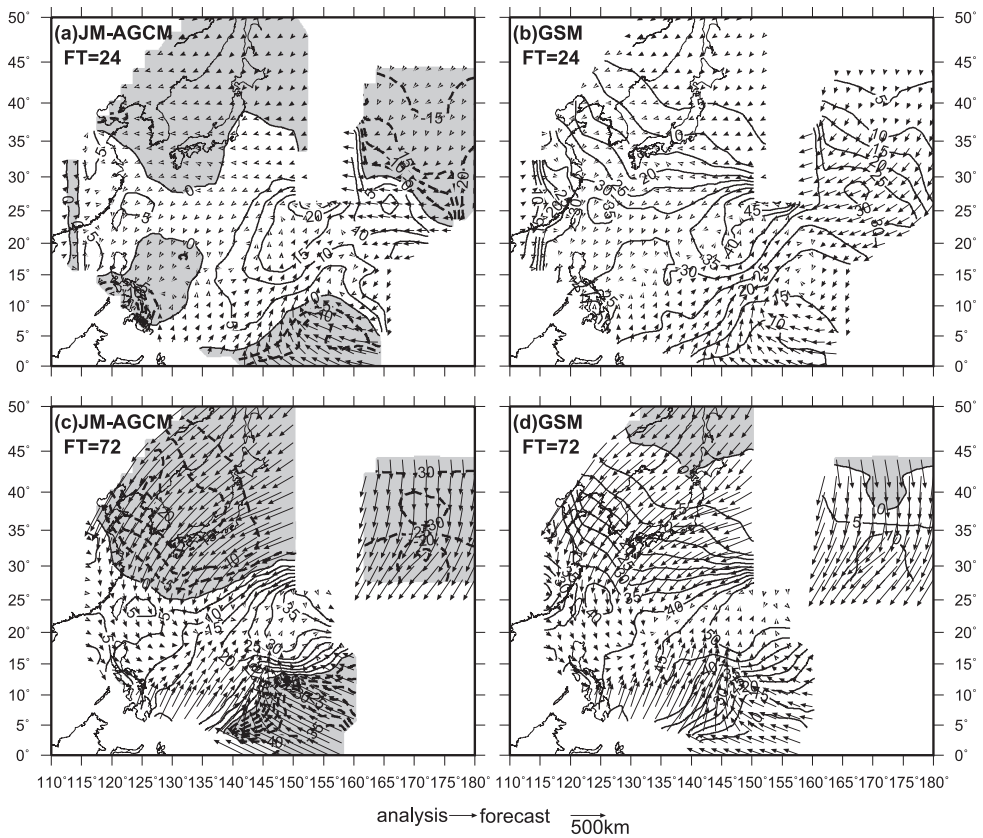

Fig. 13. Systematic bias of the mean position (vector) and sea level pressure (contour; hPa). The head, tail, and length of each arrow show the model forecast position, the best-track position, and the magnitude of the mean position error, respectively. Errors at 24 forecast hours (a) by the JM-AGCM and (b) by the GSM are shown. (c) and (d) are the same as (a) and (b) but for 72 forecast hours.

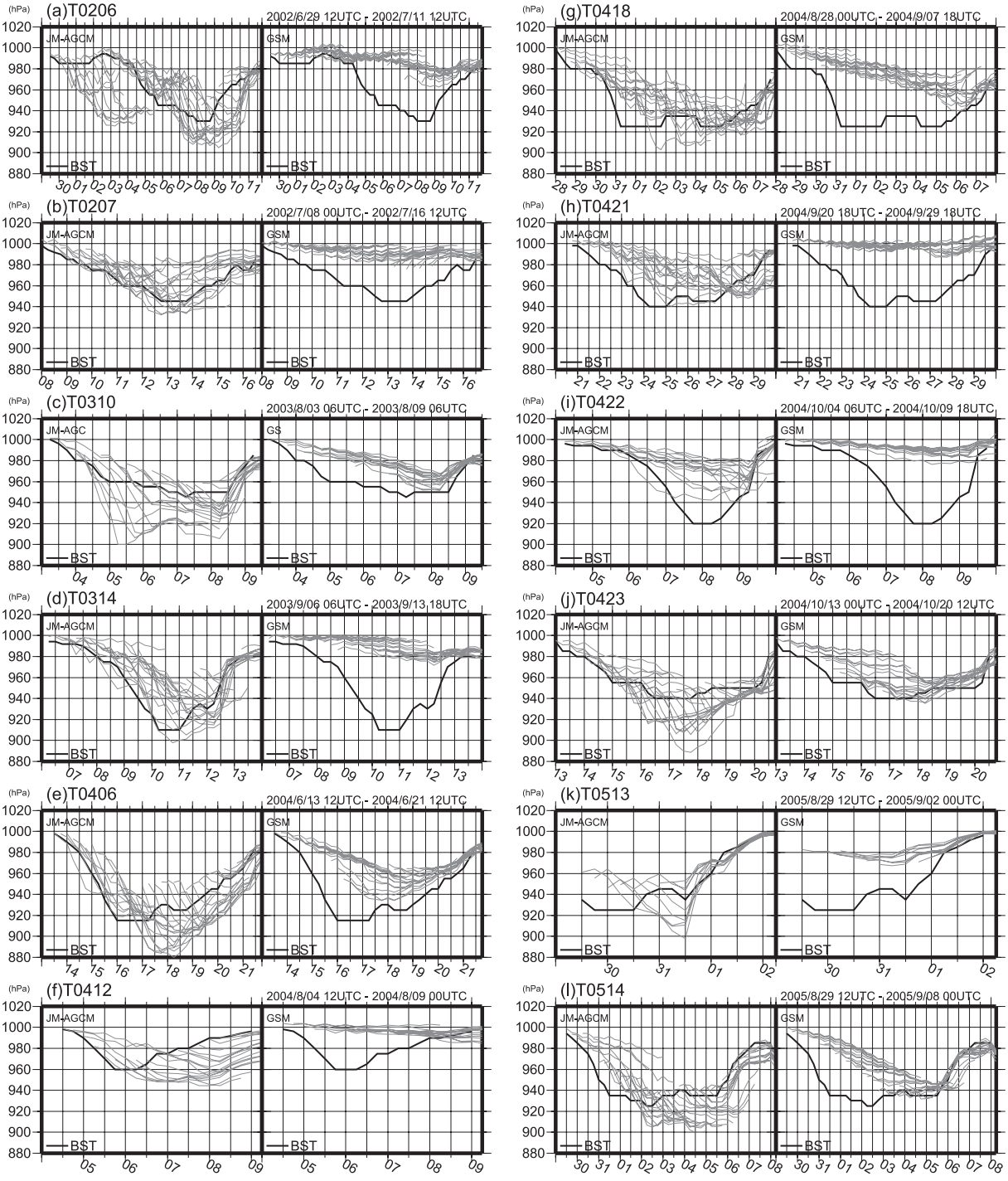

Fig. 14. Simulated typhoon central pressure by each model. For each typhoon, the left panel shows the central pressure (hPa) by the 20 km-mesh AGCM, whereas the right panel shows that by the GSM. The gray and black lines display the central pressure simulated by the best-track data and model, respectively. The numerical annotations of the abscissa denote the date.

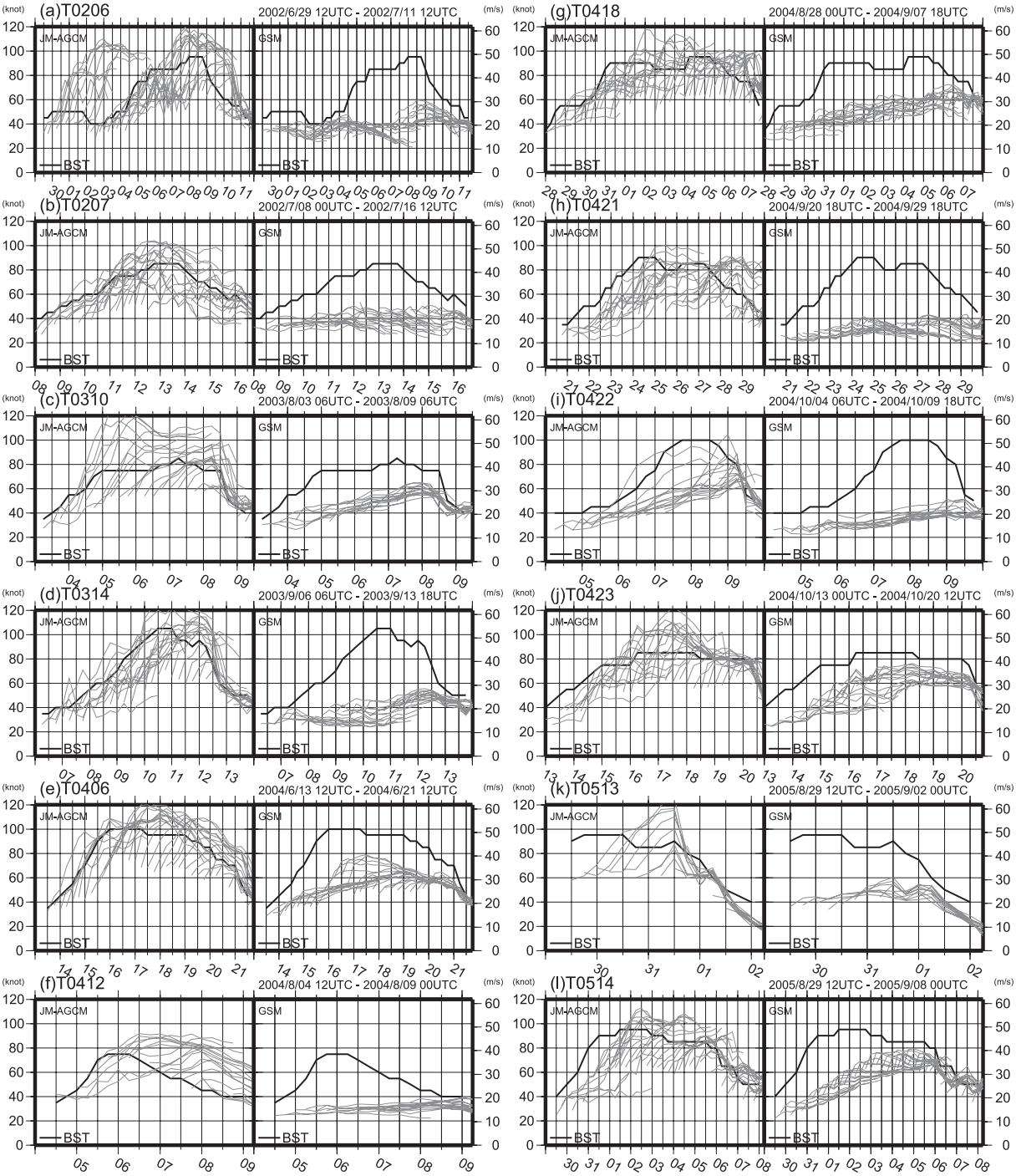

Fig. 15. Same as Fig. 14 but for the maximum sustained wind [knots]. The unit of the wind velocity that corresponds to m s^{-1} is shown in right ordinate.

to be larger than that of the GSM. It is also notable that, even in the decay stage of a typhoon, the JM-AGCM tends to increase the maximum wind and decrease the central pressure in the early forecast time and then decrease the maximum wind and increase the central pressure (see (d)T0314, (e)T0406, and (g)T0421). This insufficient tendency is mainly due to the spin-up, as described in Section 2.b. However, except for the spin-up, the JM-AGCM seems to show quite a good decaying tendency. The geographical error of central sea level pressure can be seen in Fig. 13. As a whole, the GSM shows a systematic positive bias both at (a) 24 and (c) 72 forecast hours, which is mainly due to the coarse resolution. However, the absolute error value of the JM-AGCM ((b) and (d)) is relatively smaller than that of the GSM. It is also noted that there is negative error by the JM-AGCM in the area, in which the position error is relatively large around the typhoon genesis area (between 140°E and 160°E in longitude and between 0 and 15°N in latitude) and the typhoon decaying area (northern 30°N). Although this error is likely to be mainly due to the large position error, the JM-AGCM yields an extremely low prediction of the central sea level pressure.

Figure 16 shows the tendencies of central pressure. The tendencies are evaluated by distinguishing three stages. One is the intense stage, in which the observed typhoon records a 10 hPa decrease between 24 and 72 forecast hours. Another is the steady stage, in which the observed typhoon records a decrease of between −10 hPa and 10 hPa. The other is the decay stage, in which the analyzed typhoon records a 10 hPa increase. In the intense stage, the GSM cannot simulate the typhoon deepening tendency. Most of the simulated central pressure records more than 960 hPa. This is due to the coarse resolution. The JM-AGCM, however, can simulate the deepening tendency better than the GSM. Some simulations by the JM-AGCM also reach 920 hPa, which is close to the analysis. (whether this close value is good or not for the 20 km-mesh model will be discussed later). However, it must be noted that there are some bad cases in the JM-AGCM in which the central pressure does not decrease as much as in the analysis. Although the reason for the discrepancy is uncertain, Oouchi et al. (2006) and Knutson and Tuleya (2004) suggest that it may originate in the insufficient performance of the physical scheme, including the cumulus parameterization. It may also be caused by insufficient initial condition because most of the central pressure for these cases at the 24 forecast hours (i.e., "A" in Fig. 16a) is higher than that by the observation. This insufficient typhoon structure may prevent a typhoon from intensifying. Also, in the steady stage, the JM-AGCM shows decreasing sea level pressure too much more than the observation. When this tendency is evaluated between 72 and 90 forecast hours (figure not shown), the pseudo tendency was not so strong as it is seen between 24 and 72 hours. Therefore, the insufficient typhoon structure in the initial field seems to cause such a false tendency. Although further analysis is required, it is natural to assume that the JM-AGCM has better potential than the GSM to simulate intense tendency.

For the cases of the decay stage, the JM-AGCM represents the declining tendency better than the GSM. However, some simulations show lower central pressure than the analysis at the 24 forecast hours. Those cases, in which the central pressure records less than 910 hPa by the JM-AGCM, are due to spin-up. All of the cases decrease the central pressure from the initial condition to 24 hours and then increase it from 24 hours. Except for these cases, the JM-AGCM represents the decaying tendency more adequately than the GSM. Figure 17 also shows the tendencies in the maximum wind velocity. The basic features are almost the same as the result of central pressure. It must be noted that the GSM cannot simulate an intensifying tendency that exceeds 50 knot by analysis. The JM-AGCM, however, represents the tendency more accurately than the GSM.

Overall, the JM-AGCM has better possibility than the GSM to simulates the strength tendency.

c. Typhoon structure

A comparison between the infrared image by a satellite and the expected image by simulated outputs helps to visually grasp the structure of a storm. Figure 18 is a comparison of satellite infrared image by the GOES-9 and that by model simulations. The infrared image by the model simulations is derived using a radiative transfer model based on a method in the GSM (Oowada 2006). In this case, it is conspicuous that the typhoon structure by the GSM is very vague (e.g., the eye is not resolved). On the other hand, the typhoon structure by the JM-AGCM is much finer than that by the GSM. For example, it is noted that the typhoon eye is well resolved by the JM-AGCM. The central

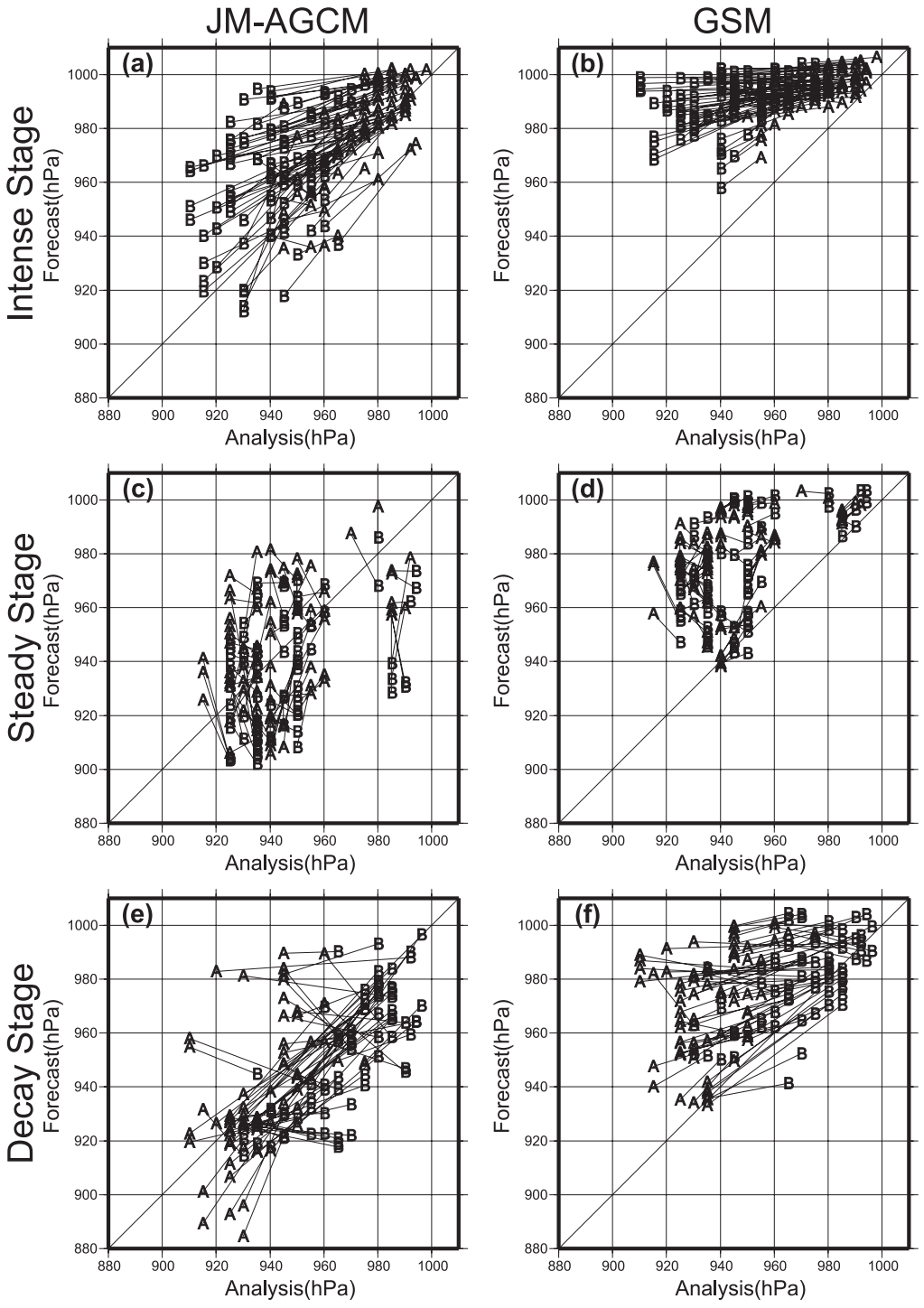

Fig. 16. Tendency of the central pressure. The unit is hPa. The ordinate is the simulated central pressure, whereas the abscissa is the corresponding central pressure of the best-track data. "A" denotes the central pressure at 24 forecast hours. "B" denotes that at 72 forecast hours. Three stages are defined as follows: (a) and (b): the intense stage, in which the observed typhoon records a 10 hPa decrease; (c) and (d): the steady stage, showing between a −10 hPa and 10 hPa decrease; (e) and (f): the decay stage, showing a 10 hPa increase. (a), (c), and (e) are according to the JM-AGCM. (b), (d), and (f) are according to the GSM.

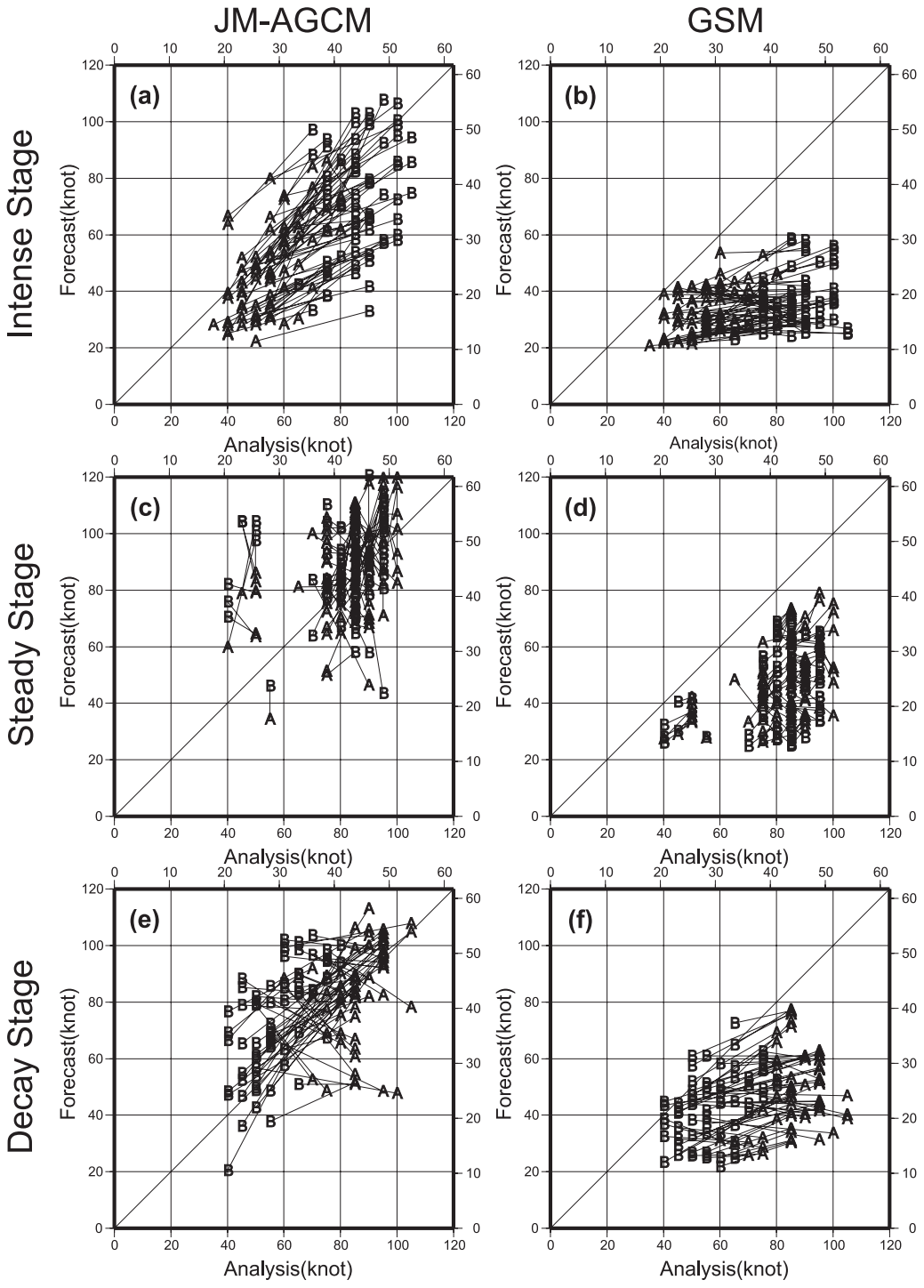

Fig. 17. Same as Fig. 16 but for the maximum wind velocity. The unit is the knot (m s^{-1} in top and right axises). The three stages are defined as follows: (a) and (b): the intense stage, in which the analyzed typhoon maximum wind velocity records a 10-knot increase; (c) and (d): the steady stage, showing between a -10-knot and a 10-knot increase; (e) and (f): the decay stage, showing 10-knot decrease.

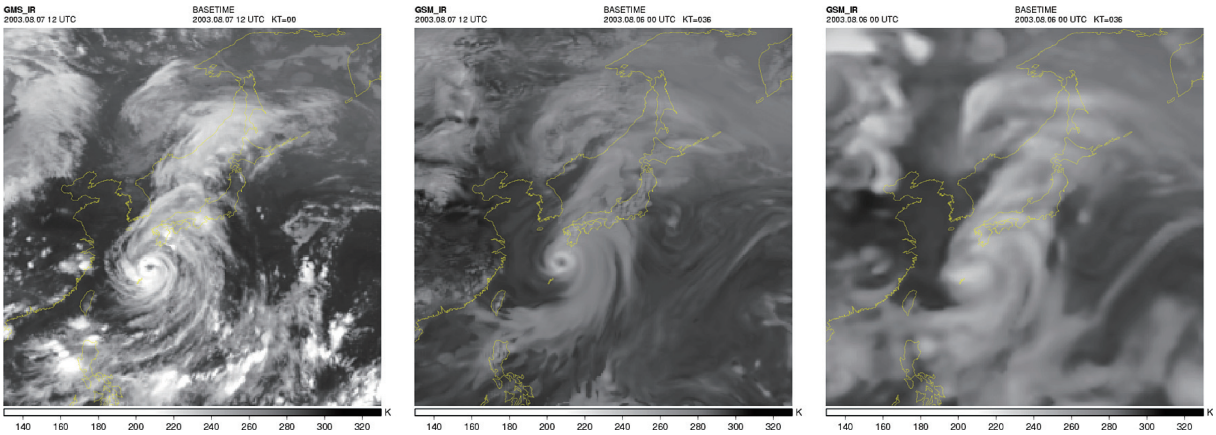

Fig. 18. Comparison of infrared images. Left: image by the GOES-9. Middle: image by the JM-AGCM. Right: image by the GSM. The typhoon of the image is the T0310. The date is 00 UTC August 06, 2003. The simulated forecast hour is 36.

pressure was 955.0 hPa, 951.0 hPa, and 966.2 hPa for the observation, the JM-AGCM, and the GSM, respectively. The eyewall is also more realistic than that by the GSM. It is also remarkable that the cloud bands of the typhoon that run from northeast to southwest are much clearer than those by the GSM. It is reasonable to suppose that the high resolution enables it to represent the typhoon structure more realistically. However, when it is compared with observation carefully, the central structure, including eyewalls, by the JM-AGCM seems to be too compact. The possible reason will be discussed later with a radial profile verification.

The simulated mean R30 and R50 are compared with those of the best-track data. Figure 19 shows the mean errors of R30 and R50. Generally, the differences between models are small. The error of R50 is, notably, almost zero or small negative bias. However, the negative bias of R30 is distinct. The negative bias means that strong winds are simulated too close to the eye of the storm. Although the error difference between the recurvature stages is small, the BR (c) stage shows relatively larger error than other stages. It is also noted that the bias in the initial condition (forecast zero hour in the Fig. 19) is relatively large compared with other forecast hours. This indicates that there is considerable room to improve the initial condition for better experiments. However, as the error of R30 is increased by the forecast hour, there are some deficiencies in the model's physical processes. As Mizuta et al. (2006) described, these errors can be alleviated by some adjustments to the physical processes.

Figure 20 shows mean wind profile for each forecast time. It is noted that the maximum wind by the JM-AGCM is located around less than 100 km from the center of storms. However, it is located between 100 km and 200 km by the GSM. Because the grid interval of GSM is 60 km, it seems to be unable to resolve such a sharp structure of wind variation around the center of a storm. It is inferred from the R30, the R50, and the maximum wind velocity by the best-track that the position of maximum wind velocity is located less than 100 km from the center, which is close to the JM-AGCM profile. It is also notable that wind structures are changed by forecast hour by the JM-AGCM, whereas those by the GSM are not changed. Although it is due to spin-up by the insufficient initial structure, the degree of spin-up is approximately alleviated after 60 forecast hours.

In order to remove the spin-up deterioration, Fig. 21 shows the same as Fig. 20, but for averaged typhoons whose maximum velocity is more than 50 knot after 60 forecast hours. It is interested that the outer-core structure, which is more than 200 km from the center, is almost the same between models. The difference is distinct in the inner-core structure. This gives us justification for the assumption that high resolution is required in order to evaluate typhoon strength, because high resolution makes it possible to capture the inner-core structure realistically.

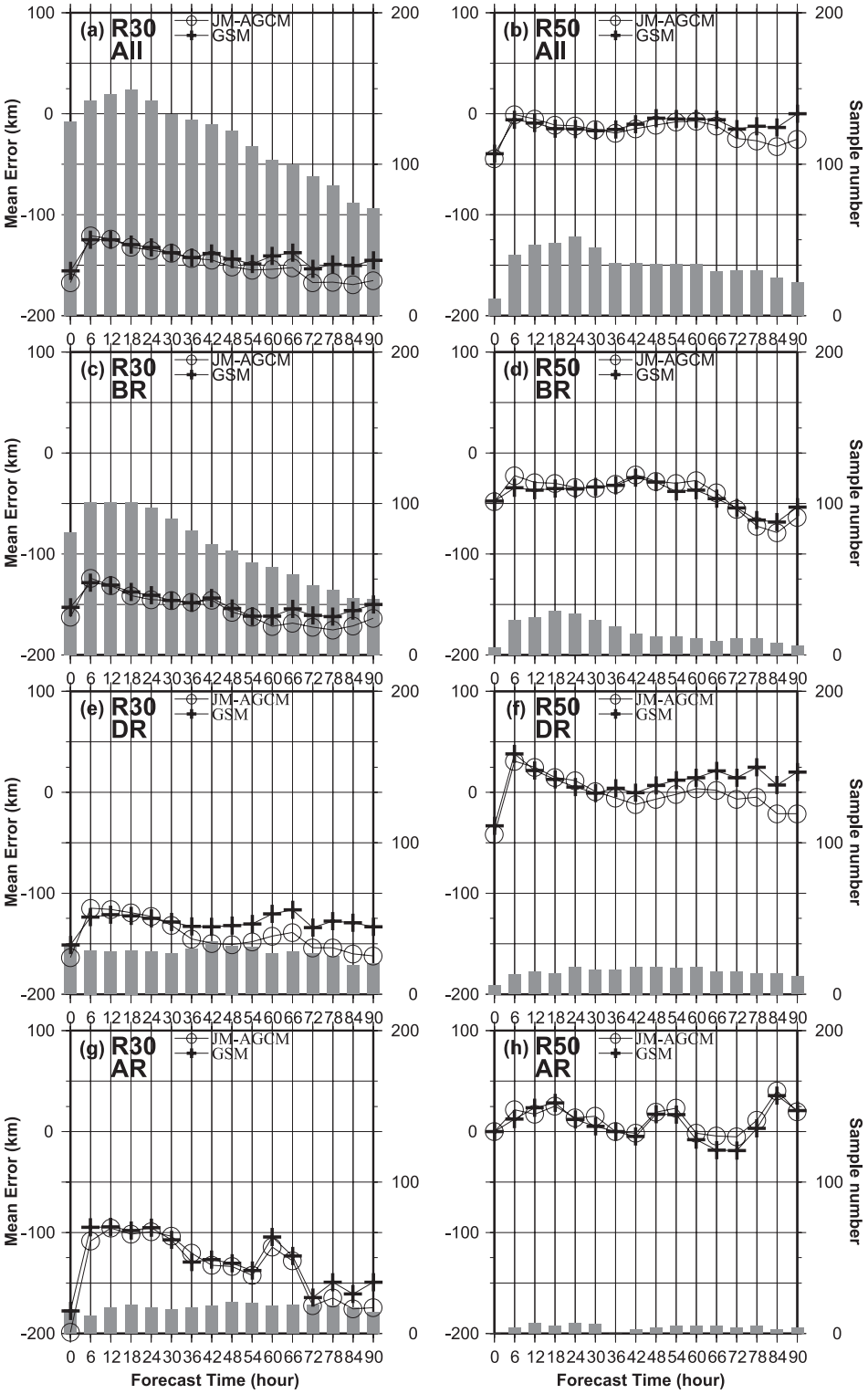

Fig. 19. Mean errors of (a) R30 and (b) R50. (c) and (d) are the same as (a) and (b) but before the recurvature; (e) and (f) are during the recurvature; (g) and (h) are after the recurvature. The legends are the same as for Fig. 8. The abscissa shows the forecast hour. The ordinate shows the mean error [km].

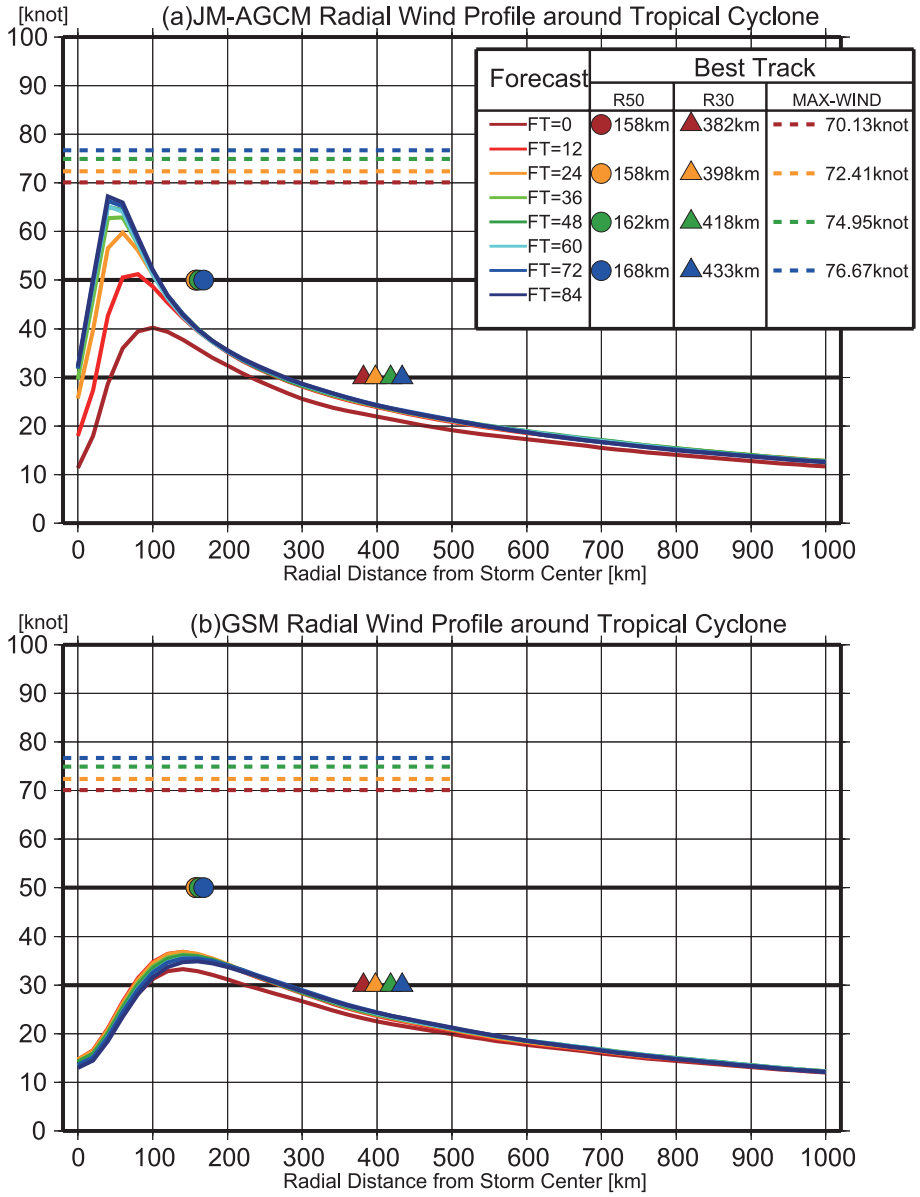

Fig. 20. Mean wind profile for each forecast time. The abscissa shows the distance from the storm center. The ordinate shows the averaged wind velocity [knot]. The colored solid lines show model results. (a) is by the JM-AGCM, and (b) is by the GSM. The circle (triangle) plots show the best-track 30 (50) knot radius, which were averaged by the corresponding forecast time. The colored broken lines show the maximum wind velocity by the best-track. (radius is unknown)

Although it appears that the JM-AGCM simulates exact structure as same as the observation as it is seen in Fig. 21, it is necessary to discuss how much resolution is enough to resolve the inner-core structure. In other words, what is the best-fitted structure as its resolution? For example, the reader might think that the structure of the JM-AGCM is too deep as its resolution. In fact, the R30 and R50 verifications show that the structure of the JM-AGCM is too more compact than the GSM at later forecast hours. The authors suppose 20km-mesh is not still enough to resolve the inner-core structure so that wind profile should be underestimated when it is compared with the observation.

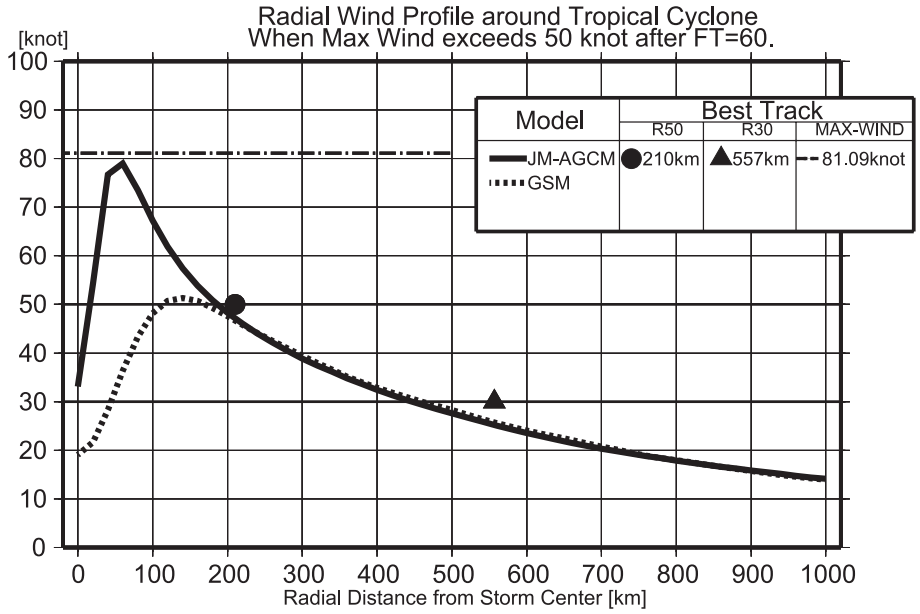

Fig. 21. Mean wind profile of storms whose wind velocity is more than 50 knot after 60 forecast hours. The abscissa shows the distance from the storm center. The ordinate shows the averaged wind velocity [knot]. The solid line shows by the JM-AGCM. The dotted line shows by the GSM. The circle (triangle) plot shows the best-track 30 (50) knot radius, which was averaged by the corresponding time. The long broken line shows the maximum wind velocity by the best-track. (radius is unknown)

Therefore it is important to evaluate the best-fitted structure as the 20km-mesh resolution. One of the hints to determine the best-fitted structure is the simulation tests with different initial typhoon bogus structures. If a spin-up is occurred as seen in the JM-AGCM case of Fig. 20, the initial structure is not considered to be the best fitted as the resolution. The initial structure of the GSM might be the best fitted as 60km mesh because spin-up is not seen. By the way, one of the possible reasons of the too compact structure might be due to the insufficient cumulus parameterization scheme (from personal communication with a JMA model developer). Both the JM-AGCM and the GSM overestimate weak precipitation which is less than 15 mm/day around tropics (Kamiguchi et al. 2006). It is indicated that shallow cumulus convection is easy to occur in the models. When this is applied to typhoon, it is inferred that deep convection does not occur easily at the outer-core side of the typhoon. As a result, shallower convection and water vapor are collected in the vicinity of the typhoon center so that deep convection is too strong around the center. For future work in order to clarify the structure error, the convection distribution conducted by a cloud resolving model may be beneficial information.

4. Summary and concluding remarks

Tropical storms over the western North Pacific Ocean were simulated by the 20km-mesh JM-AGCM. The simulations were compared with the 60km-mesh GSM as a coarse global model in order to evaluate differences in resolution. The best-track data of RSMC-Tokyo were also used as the observation data. The verification was conducted for twelve typhoon cases from 2002 to 2005. The cases were subjectively chosen. The initial conditions for the JM-AGCM simulations were insufficient because they were derived by interpolation from a 60km-mesh analysis, which resulted in false spin-ups. However, some superiority over the GSM were identified, although the statistical significance of the difference remains low because simulations were limited due to computer resources provided by the ES.

The difference in the position errors of typhoons between the JM-AGCM and the GSM is very small, although the position error of the JM-AGCM seems slightly small. The performance of

the track forecast seems to depend mainly on the large-scale flow, initial condition, and the physical process in the models rather than on the resolution difference. The statistics of the position errors are also classified into the different stages of a typhoon, namely, recurvature and intensity. The overall result is that position errors are almost identical between models. The JM-AGCM simulates the typhoon positions as realistically as the GSM. According to the analyses of the northward bias in the T0207 cases and the southward bias in the T0421 cases, schematic errors in the large-scale field, which is associated with the erroneous strength of the sub-tropical high, were found. Also, the position errors of the JM-AGCM are slightly larger than those of the GSM during the recurvature stage. This mainly comes from the erroneous intensifying tendency because of initial spin-up problem rather than from the model bias itself. The position errors are also analyzed by along/across moving direction relative to the best-track position. As a result, both models show a northward bias before the recurvature stage and a slow bias after the recurvature stage. Because there are almost the same systematic errors of large-scale field for both models, they are mainly caused by error of the physical process. As a whole, these results indicate that refining the resolution is not the only key to reduce position errors.

However, there are significant differences in intensity (maximum sustained wind and central pressure) predictions, mainly due to the resolution difference. As a whole, the GSM simulates both the central pressure and maximum wind too weekly, whereas the JM-AGCM simulates them quite realistically but somewhat too strongly. It is also remarkable that the JM-AGCM can simulate the intense or decay tendency much more realistically than the GSM. These results indicate that the JM-AGCM has better predictability on the intensity of tropical cyclones than the GSM.

The typhoon structure was also compared from the view point of the radius of 30-knot and 50-knot winds. Although both models show a similar bias, there was a negative bias in 30-knot radius, namely, the typhoon structure of the wind was too compact. However, when the composite structure of the wind profile was compared, that of inner core by the JM-AGCM shows comparatively realistic structure, which has the sharp increasing of wind velocity within 100 km in the radius. This drastic transformation of structure seems to be unable to be resolved by the GSM.

On the basis of these results, it can be concluded that the JM-AGCM simulates typhoons more realistically than the GSM in terms of intensity and inner structure. However, as the statistical significance remains low because of limited computer resources, further cases should be implemented for a future study. It is also necessary to verify other tropical cyclones over other oceans. The systematic errors, which are common in both models, namely, north bias, slow bias, and a structure of strong wind that is too compact, seem to be due to a physical process or initial conditions. It is also important to evaluate the suitable typhoon structure as the model resolution. In other words, it is insufficient to modify the typhoon structure of the model just close to that of observation; otherwise the model shows false intensity tendency and deteriorate typhoon position forecast. Further investigations and improvements with regard to these issues will be necessary for producing further reliable climate simulations and medium-range forecasts.

Acknowledgment

This work is a part of the “Kyosei Project 4: Development of Super High-Resolution Global and Regional Climate Models” supported by the Ministry of Education, Culture, Sports, Science and Technology. This work is also conducted under the framework of the “Projection of the change in future weather extremes using super-high-resolution atmospheric models” supported by KAKUSHIN Program of MEXT. The authors would like to thank Hiroto Kitagawa and Munehiko Yamaguchi of the Numerical Prediction Division of the JMA for their advice and support with regard to this study. We also thank the editor and two anonymous reviewers who provided useful comments that led to improvements of this study. The authors would also like to acknowledge the assistance and support of members of the Kyosei Project and the Numerical Prediction Division of the JMA. Thanks also go to the Earth Simulator Center for providing computational environments.

References

Arakawa, A. and W.H. Schubert, 1974: Interaction of a cumulus cloud ensemble with the large-scale environment, Part I. *J. Atmos. Sci.*, **31**, 674–701.

Ballish, B., X. Cao, E. Kalnay, and M. Kanamitsu, 1992: Incremental nonlinear normal-mode initializa-

tion. *Mon. Wea. Rev.*, **120**, 1723–1734.

Bender, M.A., R.J. Ross, R.E. Tuleya, and Y. Kurihara, 1993: Improvements in tropical cyclone track and intensity forecasts using the GFDL initialization system. *Mon. Wea. Rev.*, **121**, 2046–2061.

Bengtsson, L., M. Botzet, and M. Esch, 1996: Will greenhouse gas-induced warming over the next 50 years lead to higher frequency and greater intensity of hurricanes? *Tellus*, **48A**, 57–73.

Broccoli, A.K. and S. Manabe, 1990: Can existing climate models be used to study anthropogenic changes in tropical cyclone climate? *Geophys. Res. Lett.*, **17**, 1917–1920.

Haarsma, R.J., J.F.B. Mitchell, and C.A. Senior, 1993: Tropical disturbances in a GCM. *Clim. Dyn.*, **8**, 247–257.

Habata, S., K. Umezawa, M. Yokokawa, and S. Kitawaki, 2004: Hardware system of the Earth Simulator. *Parallel Computing*, **30**, 1287–1313.

Hamilton, K. and R.S. Hemler, 1997: Appearance of a supertyphoon in a global climate model simulation. *Bull. Amer. Meteor. Soc.*, **78**, 2874–2876.

Henderson-Sellers, A., H. Zhang, G. Berz, K. Emanuel, W. Gray, C. Landsea, G. Holland, J. Lighthill, S.-L. Shieh, P. Webster, and K. McGuffie, 1998: Tropical cyclones and global climate change: A post-IPCC assessment. *Bull. Amer. Meteor. Soc.*, **79**, 19–38.

Houghton, J.T., Y. Ding, D.J. Griggs, M. Noguer, P.J. van der Linden, and D. Xiaosu, 2001: *Climate Change 2001. The Scientific Basis*. Cambridge University Press, 944 pp.

Iwasaki, T., H. Nakano, and M. Sugi, 1987: The performance of a typhoon track prediction model with cumulus parameterization. *J. Meteor. Soc. Japan*, **65**, 555–570.

JMA, 2002: *Outline of the operational numerical weather prediction at the Japan Meteorological Agency*. 157 pp.

JMA, 2001–2005: *JMA Weather Charts*. Monthly CD-ROM.

JMA, 2007: *Outline of the operational numerical weather prediction at the Japan Meteorological Agency*. 194 pp.

Kamahori, H., N. Yamazaki, N. Mannoji, and K. Takahashi, 2006: Variability in intense tropical cyclone days in the Western North Pacific. *SOLA*, **2**, 104–107.

Kamiguchi, K., A. Kitoh, T. Uchiyama, R. Mizuta, and A. Noda, 2006: Changes in precipitation-based extremes indices due to global warming projected by a global 20-km-mesh atmospheric model. *SOLA*, **2**, 064–067.

Katayama, K., H. Yoshimura, and T. Matsumura, 2003: Development of a 20 km mesh global NWP model on the Earth Simulator. *CAS/JSC WGNE Research Activities in Atmospheric and Oceanic Modeling*, **33**, 0311–0312.

Katayama, K., H. Yoshimura, and T. Matsumura, 2004: Development of a 20 km mesh global NWP model on the Earth Simulator. *CAS/JSC WGNE Research Activities in Atmospheric and Oceanic Modeling*, **34**, 0311–0312.

Kawai, H., 2003: Impact of a cloud ice fall scheme based on an analytically integrated solution. *CAS/JSC WGNE Research Activities in Atmospheric and Oceanic Modeling*, **33**, 0411–0412.

Kawai, H., and T. Inoue, 2006: A simple parameterization scheme for subtropical marine stratocumulus. *SOLA*, **2**, 17–20.

Knutson, T.R. and R.E. Tuleya, 1999: Increased hurricane intensities with CO_2-induced warming as simulated using the GFDL hurricane prediction system. *Clim. Dyn.*, **15**, 503–519.

Knutson, T.R. and R.E. Tuleya, 2004: Impact of CO_2-induced warming on simulated hurricane intensity and precipitation: Sensitivity to the choice of climate model and convective parameterization. *J. Climate*, **17**, 3477–3495.

Knutson, T.R., R.E. Tuleya, and Y. Kurihara, 1998: Simulated increase of hurricane intensities in a CO_2-warmed climate. *Science*, **279**, 1018–1020.

Krishnamurti, T.N., R. Correa-Torres, and N. Dignon, 1998: The impact of current and possibly future sea surface temperature anomalies on the frequency of Atlantic hurricanes. *Tellus*, **50A**, 186–210.

Kurihara, Y., M.A. Bender, and R.J. Ross, 1993: An initialization scheme of hurricane models by vortex specification. *Mon. Wea. Rev.*, **121**, 2030–2045.

Kusunoki, S., J. Yoshimura, H. Yoshimura, A. Noda, K. Oouchi, and R. Mizuta, 2006: Change of Baiu rain band in global warming projection by an atmospheric general circulation model with a 20-km grid size. *J. Meteor. Soc. Japan*, **84**, 581–611.

Landsea, C.W., B.A. Harper, K. Hoarau, and J.A. Knaff, 2006: Can we detect trends in extreme tropical cyclones? *Science*, **313**, 452–454.

Levinson, D.H., 2005: State of the climate in 2004. *Bull. Amer. Meteor. Soc.*, **86**, S1–S86.

Mellor, G.L. and T. Yamada, 1974: A hierarchy of turbulence closure models for planetary boundary layers. *J. Atmos. Sci.*, **31**, 1791–1806.

Mizuta, R., K. Oouchi, H. Yoshimura, A. Noda, K. Katayama, S. Yukimoto, M. Hosaka, S. Kusunoki, H. Kawai, and M. Nakagawa, 2006: 20-km-mesh global climate simulations using JMA-GSM model –mean climate states–. *J. Meteor. Soc. Japan*, **84**, 165–185.

Murai, S. and S. Yabu, 2005: Introduction of a new radiation scheme to the operational global NWP model at JMA. *CAS/JSC WGNE Research Activities in Atmospheric and Oceanic Modeling*, **35**, 0419–0420.

Murakami, H. and T. Matsumura, 2007: Development of an effective non-linear normal mode initialization method for a high resolution global model. *J. Meteor. Soc. Japan*, **85**, 187–208.

Nakagawa, M., 2003: Development of a cumulus parameterization scheme of the operational global model at JMA. *CAS/JSC WGNE Research Activities in Atmospheric and Oceanic Modeling*, **33**, 0417–0418.

Ohfuchi, W., H. Nakamura, M.K. Yoshioka, T. Enomoto, K. Takaya, X. Peng, S. Yamane, T. Nishimura, Y. Kurihara, and K. Ninomiya, 10-km mesh mesoscale resolving simulations of the global atmosphere on the Earth Simulator –preliminary outcomes of AFES (AGCM for the Earth Simulator)– *J. Earth Simulator*, **1**, 8–34.

Oouchi, K., J. Yoshimura, H. Yoshimura, R. Mizuta, S. Kusunoki, and A. Noda, 2006: Tropical cyclone climatology in a global-warming climate as simulated in a 20km-mesh global atmospheric model: Frequency and wind intensity analyses. *J. Meteor. Soc. Japan*, **84**, 259–276.

Oowada, H., 2006: Satellite forecasted image. *Meteor. Res. Notes* **212**, 140, (in Japanese).

Royer, J.-F., F. Chauvin, B. Timbal, P. Araspin, and D. Grimal, 1998: A GCM study of the impact of greenhouse gas increase on the frequency of occurrence of tropical cyclones. *Clim. Change*, **38**, 307–343.

Sakai, R. and M. Yamaguchi, 2005: The WGNE intercomparison of tropical cyclone track forecasts by operational global models. *CAS/JSC WGNE Research Activities in Atmospheric and Oceanic Modeling*, **35**, 0207–0208.

Schmidlin, T.W., 2006: On evacuation and deaths from Hurricane Katrina. *Bull. Amer. Meteor. Soc.*, **87**, 754–756.

Shapiro, L.J. and S.B. Goldenberg, 1998: Atlantic sea surface temperatures and tropical cyclone formation. *J. Climate*, **11**, 578–590.

Shen, B.-W., R. Atlas, O. Reale, S.-J. Lin, J.-D. Chern, J. Chang, C. Henze, and J.-L. Li, 2006: Hurricane forecasts with a global mesoscale-resolving model: Preliminary results with Hurricane Katrina (2005). *Geophys. Res. Lett.*, **33**, L13813.

Simmons, A.J. and D.M. Burridge, 1981: An energy and angular-momentum conserving vertical finite-difference scheme and hybrid vertical coordinates. *Mon. Wea. Rev.*, **109**, 758–766.

Sugi, M., A. Noda, and N. Sato, 2002: Influence of the global warming on tropical cyclone climatology: An experiment with the JMA global model. *J. Meteor. Soc. Japan*, **80**, 249–272.

Tokuno, M. and Y. Ohhashi, 2003: Assimilation of QuikSCAT/SeaWinds ocean surface wind data into the global data assimilation system at JMA. *CAS/JSC WGNE Research Activities in Atmospheric and Oceanic Modeling*, **33**, 0137–0138.

Tsutsui, J., 2002: Implications of anthropogenic climate change for tropical cyclone activity: A case study with the NCAR CCM2. *J. Meteor. Soc. Japan*, **80**, 45–65.

Ueno, M., 1995: A study on the impact of asymmetric components around tropical cyclone center on the accuracy of bogus data and the track forecast. *Meteo. Atmos. Phys.*, **56**, 125–134.

Walsh, K.J.E. and B.F. Ryan, 2000: Tropical cyclone intensity increase near Australia as a result of climate change. *J. Climate*, **13**, 3237–3254.

Webster, P.J., G.J. Holland, J.A. Curry, and H.-R. Chang, 2005: Changes in tropical cyclone number, duration, and intensity in a warming environment. *Science*, **309**, 1844–1846.

WMO, 2005: Typhoon committee operational manual –meteorological component–, WMO/TD 196, World Meteorological Organization.

Wu, C.-C., M.A. Bender, and Y. Kurihara, 2000: Typhoon forecast with the GFDL hurricane model: Forecast skill and comparison of predictions using AVN and NOGAPS global analyses. *J. Meteor. Soc. Japan*, **78**, 777–788.

Yoshimura, H. and T. Matsumura, 2003: A semi-Lagrangian scheme conservative in the vertical direction. *CAS/JSC WGNE Research Activities in Atmospheric and Oceanic Modeling*, **33**, 0319–0320.